Genetic Analysis of the Organization, Development, and Plasticity of Corneal Innervation in Mice

Nacim Bouheraoua, Stéphane Fouquet, Maria Teresa Marcos-Almaraz, Domna Karagogeos, Laurent Laroche, Alain Chédotal

Genetic analysis of the organization, development and plasticity of corneal innervation in mice.

Nacim Bouheraoua[1, 2*], Stéphane Fouquet[1], Maria Teresa Marcos Almaraz[1], Domna Karagogeos[3], Laurent Laroche[1, 2] and Alain Chédotal[1*]

[1]Institut de la Vision, Sorbonne Université, INSERM, CNRS, 17 Rue Moreau, F-75012 Paris, France.

[2]Quinze-Vingts National Ophthalmology Hospital, Sorbonne Université, DHU Sight Restore, INSERM-DGOS CIC 1423, 28 rue de Charenton, F-75012 Paris, France

[3]Department of Basic Science, Faculty of Medicine, University of Crete, Vassilika Vouton, Heraklion, Crete 71110, Greece

[*]**Corresponding authors**: alain.chedotal@inserm.fr; nacim.bouheraoua@gmail.com

Short title: A genetic toolbox for studying cornea innervation

Number of pages : 43 **; Number of figures**: 10**; Number of words:** Abstract (218), Introduction (521) , Discussion (1115)

The authors declare no competing financial interests

Acknowledgements: This work was supported by the Institut de Recherche Ophtalmologique de Paris (to N.B.). We thank Dr Jean Livet for providing the Brainbow line.

Author contribution: AC, NB and LL designed research. NB, SF and MTMA performed research. DG and DK contributed reagents/analytic tools. SF and NB analyzed data. AC and NB wrote the paper. AC, NB and SF prepared the figures. All authors revised the manuscript.

Journal section: Development/Plasticity/Repair

Keywords: Cornea; neuropilin; corneal nerves; corneal innervation; mouse

Abstract

The cornea has the densest sensory innervation of the body, originating primarily from neurons in the trigeminal ganglion. The basic principles of cornea nerve patterning have been established many years ago using classic neuroanatomical methods such as immunocytochemistry and electrophysiology. Our understanding of the morphology and distribution of the sensory nerves in the skin has considerably progressed over the past few years through the generation and analysis of a variety of genetically modified mouse lines. Surprisingly, these lines were not used to study corneal axons. Here, we have screened a collection of transgenic and knockin mice (of both sexes) to select lines allowing the visualization and genetic manipulation of corneal nerves. We identified multiple lines, including some in which different types of corneal axons can be simultaneously observed with fluorescent proteins expressed in a combinatorial manner. We also provide the first description of the morphology and arborization of single corneal axons and identify three main types of branching pattern. We applied this genetic strategy to the analysis of corneal nerve development and plasticity. We provide direct evidence for a progressive reduction of the density of corneal innervation during aging. We also show that the semaphorin receptor neuropilin-1 acts cell-autonomously to control the development of corneal axons and that early axon guidance defects have long-term consequences on corneal innervation.

Significance statement : We have screened a collection of transgenic and knockin mice and identify lines allowing the visualization and genetic manipulation of corneal nerves. We provide the first description of the arborization pattern of single corneal axons. We also present applications of this genetic strategy to the analysis of corneal nerve development and remodeling during aging

Introduction

The somatosensory system conveys a variety of stimuli such as pressure, temperature and pain, transmitted to the central nervous system by a myriad of sensory axons that project to most organs including the skin. The cornea epithelium, receives sensory inputs via the ophthalmic branch of the trigeminal nerve and is the densest innervated tissue at the surface of the body (Rózsa and Beuerman, 1982; Marfurt et al., 1989; Müller et al., 2003; Belmonte et al., 2015). The cornea is also innervated by autonomic axons coming from the ciliary and superior cervical ganglia, representing only 5-10% of the corneal axons (Marfurt and Ellis, 1993).

The properties and organization of corneal nerves have been studied for decades with a wide range of techniques. Electrophysiological studies have shown that the cornea is innervated by A-delta (myelinated) and C-fiber (unmyelinated) afferents (Lele and Weddell, 1959) comprising three functional classes : pure mechano-nociceptors, cold sensing neurons and polymodal nociceptors (Belmonte et al., 1991; González-González et al., 2017) responding to various noxious stimuli (mechanical, thermal and chemical). Corneal axons have been visualized in humans and mice using Golgi staining, axonal tracing, lectin binding (Zander and Weddell, 1951; Marfurt, 1988; de Castro et al., 1998) as well as non-invasive confocal laser scanning microscopy (Reichard et al., 2014; Ehmke et al., 2016). More recently, evidence for a higher diversity of corneal nerves has emerged through the characterization of receptors transducing the various sensory modalities in corneal axons, such as TRPV1 and TRPA1 (transient receptor potential cation channels subfamilies V or A, member 1) for heat and chemical agents (Caterina et al., 1997; Nakamura et al., 2007; Alamri et al., 2015; Canner et al., 2015), Piezo2 for mechanical forces (Coste et al., 2010; Bron et al., 2014; Ranade et al., 2014) and TRPM8 (transient receptor potential cation channel subfamily M member 8) for cold (Bautista et al., 2007; Parra et al., 2010; Quallo et al., 2015). A few markers of corneal

nerves have been validated with immunolabeling procedures, such as anti-ßIII-tubulin or anti-PGP95 which recognize all types of corneal axons, or anti-CGRP, which only label some specific subsets (Marfurt et al., 2001; Murata and Masuko, 2006; Shimizu et al., 2007; Alamri et al., 2015). However, the analysis of the respective distribution and morphology of the different type of axons mediating different modalities, their development and responses to injury has been hampered by technical problems such as an incomplete antibody penetration in the thickness of the cornea.

Recently, huge progress has been made in our understanding of the sensory innervation of the hairy skin through the use of genetically modified mouse lines expressing fluorescent proteins or cre recombinase, in specific subsets of axons (Abraira and Ginty, 2013; Le Pichon and Chesler, 2014; Rutlin et al., 2014; Zimmerman et al., 2014). Surprisingly, only two transgenic lines have been used so far to study corneal nerves and few corneal nerve-cre lines have been described (Namavari et al., 2011; Omoto et al., 2012; Parra et al., 2010; Yu and Rosenblatt, 2007). Here, we have screened a collection of transgenic and knockin mice to identify lines allowing the visualization and genetic manipulation of corneal nerves.

Methods

Mouse lines

Mice of either sex were used. All lines were previously described and were genotyped by PCR: *Neuropilin1*^{lox} (Gu et al., 2003), *CAG:cre*^{ERT2} (Guo et al., 2002), *En1:cre* (Kimmel et al., 2000), *Islet1:cre* (Yang et al., 2006), *Ret:cre*^{ERT2} (Luo et al., 2009), *Split:cre* (Rutlin et al., 2014), *TAG-1:cre* (Schmidt et al., 2014), *Wnt1:cre* (Danielian et al., 1998), *CGRP:GFP* (Gong et al., 2003) *MrgprD:GFP* (Zylka et al., 2005), *Npy2r:GFP* (Li et al., 2011), *Rosa*^{tdTomato} (Madisen et al., 2010), *Tau*^{GFP} (Hippenmeyer et al., 2005), *Tau*$^{Syn\text{-}GFP}$ (Esposito et al., 2014), *Thy1:Brainbow1.0* (Livet et al., 2007), *TrkB:TauGFP* (Li et al., 2011),

VGlut3:GFP (Seal et al., 2009). Wild-type mice were from the C57BL6 background (Janvier, France). Compound mutants were obtained by intercrossing the various lines. The day of the vaginal plug was counted as E0.5 and the day of the birth as postnatal day 0 (P0). All animal procedures were carried out in accordance with the European Community Council directive (86/609/EEC) for the care and use of laboratory animals and approved by the Sorbonne Université ethics committee (comité Charles Darwin).

Tamoxifen administration

Adult (2 month-old) *Ret:cre^{ER};Rosa^{Tom}*, *Ret:cre^{ER};Tau^{GFP}*, *Ret:cre^{ER};Rosa^{Tom};Tau^{GFP}*, *Ret:cre^{ER};Rosa^{Tom};CGRP:GFP and CAG:cre^{ERT2};Thy1-Brainbow1.0* mice were injected intraperitoneally with a single dose (ranging from 0.25 mg to 3 mg) of tamoxifen (Sigma-Aldrich, T-5648) dissolved in corn oil (Sigma-Aldrich, C-8267). Animals were perfused and tissue collected, 14 days to 60 days later. P0 pups of *CAG:cre^{ERT2};Thy1-Brainbow1.0* were subcutaneously injected with 0.3mg of tamoxifen.

Immunohistochemistry

The primary and secondary antibodies used are listed in Table 1.

Cornea

Mice were euthanized and the eyeballs were enucleated and fixed in freshly prepared 4% paraformaldehyde for 15 minutes. Next, the corneas were carefully excised along the sclerocorneal rim and fixed for an additional 45 minutes, followed by three washes with PBS. To block nonspecific binding, corneas were placed in a 96-well plate (one cornea/well) and then incubated with 0.2% gelatin in PBS containing 0.5% Triton-X100 (Sigma) for 60 minutes at room temperature. The tissue was then incubated with primary antibodies for 72

hours at room temperature. After washing with PBS the corneas were incubated in species specific secondary antibodies directly conjugated to fluorophores (see Table 1) for 24 hours at room temperature and then washed thoroughly with 0.1 M PBS.

Corneas were examined using a fluorescent microscope (DM6000, Leica Microsystems) equipped with a CoolSnapHQ camera (Princeton Instruments, Trenton, NJ) or a confocal microscope (FV1000, Olympus, Japan). Brightness and contrast were adjusted using Adobe Photoshop CS6 software (RRID:SCR_014199).

Trigeminal ganglia

Adult mice were anesthetized with ketamine (50 mg/kg) and xylazine (10 mg/kg) intraperitoneally and perfused using 4% paraformaldehyde in 0.1 M phosphate buffer (PFA), pH 7.4. The crania was opened, and both left and right trigeminal ganglia (TG) were removed and fixed in freshly prepared 4% paraformaldehyde for 1 hour, followed by three washes with 0.1M PBS. Samples were cryoprotected in a solution of 10% sucrose in 0.12M phosphate buffer (pH7.2), frozen in isopentane at -50°C and then cut at 20µm with a cryostat (Leica). Immunohistochemistry was performed on cryostat sections after blocking in 0.2% gelatin in PBS containing 0.25% Triton-X100 (Sigma). Sections were then incubated overnight at room temperature with the primary antibodies (Table 1). After washing with PBS the sections were incubated at room temperature in species specific secondary antibodies directly conjugated to fluorophores for 2 hours and then washed thoroughly with 0.1 M PBS. Nuclei were counterstained using DAPI (4',6-Diamidino-2-Phenylindole, Dilactate; 1:1000; Thermo Fisher). Sections were examined using a fluorescent microscope (DM6000, Leica Microsystems) equipped with a CoolSnapHQ camera (Princeton Instruments, Trenton, NJ), a confocal microscope (FV1000, Olympus, Japan), or a slide scanner (Nanozoomer,

Hamamatsu, Japan). Brightness and contrast were adjusted using Adobe Photoshop CS6 software.

Confocal microscope acquisition

Imaging

Cornea image stacks were acquired with an Olympus FV1000 laser-scanning confocal microscope. The objectives used were an Olympus UPLSAPO 4X NA 0.16 WD 13, UPLSAPO 10X NA 0.4 WD 3.1, XLUMPPLFL 10X NA 0.6 WD 3.1, UPLSAPO 20X NA 0.85 WD 0.20, UPLFLN 40X NA 1.30 WD 0.20, PLAPON 60X SC NA 1.40 WD 0.12, or UPLSAPO 100X NA 1.4 WD 0.13.

DAPI, eCFP, AlexaFluor-594 (or RFP), AlexaFluor-647 and AlexaFluor-488 (or eGFP), eYFP, were excited using 405 nm, 440 nm, 559 nm, 635 nm laser diodes lines and 488-515 nm argon ion laser lines, respectively. Controls of the microscope and image acquisition were conducted with Olympus Fluoview software version 4.2. Image acquisition was conducted at a resolution of 1024×1024 pixels, with a scan rate of 8 to 10 $\mu s.pixel^{-1}$ and with or without zoom. Images were acquired sequentially, line by line, in order to reduce excitation and emission crosstalk, step size was defined according to the Nyquist-Shannon sampling theorem. Exposure settings that minimized oversaturated pixels in the final images were used. When acquiring images to be stitched, the MATL module from Fluoview software was used to program 10% overlap between each tiles. Montage was then processed using Fluoview software or ImageJ stitching plugins (Preibisch et al., 2009).

Image processing

To change orientation and to obtain sagittal view of the stacks, a resampling was processed using the reslice option of ImageJ software. Twelve bit images were processed with ImageJ

(RRID:SCR_003070) or FIJI (RRID:SCR_002285), Z-sections were projected on a single plane using maximum intensity under Z-project function. Images were finally converted into 24 bits RGB color mode and figures were then assembled by using Adobe Photoshop CS6. To improve contrast, a negative image of the fluorescent axons was sometimes generated using Photoshop (Adobe) or Imaris software (version 8.4.1, Bitplane). In this case, axons appeared in black on a white background.

For 3D rendering, images were generated using Imaris. Stack images were first converted to imaris file format (.ims) using ImarisFileConverter and 3D reconstruction was performed using the “volume rendering” function. To facilitate image processing, images were converted to an 8-bits format. Optical slices were obtained using the “orthoslicer” tool. 3D pictures and movies were generated using the “snapshot” and “animation” tools.

Automated tracking of cornea nerves:

Imaris filament tracer tool was used to draw and isolate unique axons on confocal images. Filaments were first rendered by manually selecting dentrite starting point, the filaments were then traced and volume rendered using the AutoDepth algorithm and represented as cylinders (2µm/filament). Following this tracing step, cornea nerve morphology was observed, tracing comptabilized and different type of nerve terminals were classified

3DISCO tissue clearing and 3D light sheet microscopy

Embryos

Whole embryos were fixed by immersion in 4% PFA overnight at 4°C. Samples were first incubated at room temperature on a rotating shaker in a solution (PBSGT) of PBS 1X containing 0.2% gelatin (Prolabo), 0.5% Triton X-100 (Sigma-Aldrich) and 0.01% thimerosal (Sigma-Aldrich) for 3 hr. Samples were next transferred to PBSGT containing the primary

antibody (goat anti-Tag-1; 1:500; R&D Systems) and placed at 37 C°, with rotation at 100 rpm, for 3 days. This was followed by six washes of 30 min in PBSGT 0.5% at room temperature. Next, samples were incubated in secondary antibodies diluted in PBSGT 0.5% (Table 1) overnight at room temperature. After six washes of 30 min in PBSGT 0.5%, samples were stored at 4°C in PBS until clearing.

3DISCO clearing

For tissue clearing, a modified 3DISCO protocol was used (Belle et al., 2014). First, embryos were fixed by immersion in 4% paraformaldehyde in 0.12 M phosphate buffer, pH 7.4 (PFA) overnight at 4°C. All incubation steps were performed in dark conditions at room temperature in a fume hood, on a tube rotator (SB3, Stuart) at 14 rpm, using a 15 mL centrifuge tube (TPP, Dutscher). Samples were first dehydrated in ascending concentrations (50%, 80%, and 100%) of tetrahydrofuran (THF; anhydrous, containing 250 ppm butylated hydroxytoluene inhibitor, Sigma-Aldrich) diluted in H_2O. The initial 50% THF bath was done overnight while the 80% and 100% THF incubations were left for 1.5 hr each. Samples next underwent a delipidation step of 30 min in dichloromethane (DCM; Sigma-Aldrich) followed by an overnight clearing step in dibenzyl ether (DBE; Sigma-Aldrich). The next day, samples were stored in individual light-absorbing glass vials (Rotilabo, Roth) at room temperature.

3D imaging

Acquisitions were performed using a light sheet fluorescence microsope (Ultramicroscope I, LaVision BioTec) with the ImspectorPro software (LaVision BioTec). The light sheet was generated by a laser (640nm wavelength, Coherent Sapphire Laser, LaVision BioTec) and focused using two cylindrical lenses. Two adjustable protective lenses were applied for small and large working distances. A binocular stereomicroscope (MXV10, Olympus) with a 2x objective (MVPLAPO, Olympus) was used at 2.5x and 3.2x. Samples were placed in an

imaging reservoir made of 100% quartz (LaVision BioTec) filled with DBE and illuminated from the side by the laser light. A PCO Edge SCMOS CCD camera (2,560 × 2,160 pixel size, LaVision BioTec) was used to acquire images. The step size between each image was fixed at 1 and 2 µm. All tiff images are generated in 16-bits.

Experimental design and statistical analysis

Statistical analyses of the mean and variance were performed with Prism 7 (GraphPad Software; RRID:SCR_002798). Mice of either sex were used throughout the studies. Results are presented as mean ± standard deviation for continuous variables and as proportions (%) for categoric variables. The Kruskal-Wallis test and the Mann-Whitney test were used to compare continuous data as appropriate. The nerve fiber length was calculated as the total length nerve fibers and branches on a maximal projection of the ultramicroscope image. Quantification was performed using NeuronJ (RRID:SCR_002074), a semiautomated nerve analysis plug-in program of ImageJ. Fiber density was quantified by measuring pixel density in a cornea field of 300 µm x 300 µm (corresponding to a 40x objective) using Image J. In some cases, the epithelium and stroma were isolated using the orthoslicer tool of Image J and next the density of corneal axons in each layer was quantified. The central zone was defined by a radius of 0.5 mm starting at the apex, and the peripheral zone with a radius of 0.5 mm beginning at the limbus. The structure of the cornea in *Tag1:Cre;Npn1^{lox}* mice, was studied using DAPI counterstaining. We used the cell counter tool and the measurement tool (Image J) to quantified the number of superficial epithelial cells, basal epithelial cells, and keratocytes and corneal thickness. Differences were considered significant when $P < 0.05$.

Results

A unique collection of transgenic lines for visualizing corneal nerves

CGRP:GFP line

In the cornea of rodents, most peptidergic nociceptive C-fibers are immunoreactive for CGRP and almost two thirds of trigeminal neurons are CGRP+ (Jones and Marfurt, 1991; Ivanusic et al., 2013; He and Bazan, 2016). However, a comprehensive map of GGRP innervation in the mouse cornea was only recently generated using whole-mount immunostaining (Alamri et al., 2015; He and Bazan, 2016). To try visualizing CGRP+ axons without immunostaining, we used a BAC transgenic (Figure 1A; see methods) which was previously shown to label C-fibers and a few Aß-Low threshold mechanoreceptors (LTMRs) in the mouse hairy skin (Bai et al., 2015). Whole-mount corneas were dissected, flat-mounted and imaged with a confocal microscope revealing a dense network of GFP+ axons covering the cornea (Figure 1B; n >30). We next performed whole-mount immunolabeling of some corneas (n=3) with anti-GFP antibodies to determine if the endogenous GFP fluorescence signal faithfully reflected the population of axons expressing the reporter. Secondary antibodies coupled to Alexa-Cy3 were used to distinguish endogenous fluorescence from GFP-immunostaining. Confocal imaging showed that direct GFP fluorescence signal perfectly matched the GFP immunostaining (Figure 1C). Reslicing of the image stacks using ImageJ (see methods) allowed following corneal nerves and axons in the stroma, subbasal plexus to their arborizations and endings in the cornea epihelium (Figure 1D). Whole-mount immunostaining for CGRP (n=3 corneas) showed that all CGRP+ axons co-expressed GFP (Figure 1E). Some GFP+ axons did not appear to be CGRP+, but this was probably due to the incomplete penetration of the anti-CGRP antibodies. Next, the trigeminal ganglia of CGRP:GFP mice (n=5) was cut with a cryostat and immunostained with anti-ßIII-Tubulin, a pan-neuronal marker. As expected, this showed that only a subset of trigeminal neurons express GFP (36 ± 2.4 %) (Figure 1F).

Accordingly, in corneas immuno-labelled for ßIII-Tubulin, the GFP+ axons only represented a fraction of the ßIII-Tubulin+ axons (Figure 1G). CGRP+ fibers represent 64% of the ßIII-Tubulin+ fibers in the center of the cornea (94060 ± 14684 pixels CGRP+ *vs* 146351 + 27062

pixels ßIII+) and 56% of the ßIII-Tubulin+ fibers in the periphery of the cornea (69314 ± 13702 pixels CGRP+ vs 123187 ± 14238 pixels ßIII+).

Finally we found that CGRP+ axons were significantly fewer in the periphery than in the center of the cornea (p=0.04; Mann-Withney test) and represented about two-thirds of adult corneal axons consistently with previous studies (He and Bazan, 2016).

To determine if the *CGRP:GFP* line could be used to study the development of corneal peptidergic axons, corneas from P0 and P10 *CGRP:GFP* mice were collected and double immunostained for ßIII-Tubulin and GFP (n=5 and n=8, respectively). At P0, GFP+ axons could be directly observed but they were more numerous and more strongly labelled after anti-GFP immunostaining (Figure 1H) suggesting that transgene expression is weaker at birth than in adults. However, at P10 the endogenous GFP signal in corneal nerves appeared as intense as in adults (Figure 1I). Both at P0 and P10, GFP+ axons co-expressed ßIII-Tubulin but they only represented a fraction of the corneal axons (Figures 1H, I). Together, these data suggest that the dense network of nociceptive peptidergic C-fibers can be fully imaged using the *CGRP:GFP* line.

Wnt1:cre line

Genetic fate-mapping studies have demonstrated that sensory neurons in the trigeminal ganglia derive from the trigeminal placode and from neural crest cell progenitors in the dorsal neural tube (Steventon et al., 2014) expressing the Wnt1 transcription factor (Evans and Gage, 2005). The *Wnt1:cre* line, was previously used to permanently label neural crest cell derivatives (Danielian et al., 1998; Gage et al., 2005). To try visualizing trigeminal neuron projections to the cornea, we crossed *Wnt1:cre* mice (Danielian et al., 1998) to two reporter lines (Figure 2A). First, we use the *Rosa26:tdTomato* line (*Rosa*^{Tom}) in which the red fluorescent protein Tomato is expressed upon Cre recombinase activity (Madisen et al., 2010); In corneas from *Wnt1:cre;Rosa*^{Tom} mice (n=2), numerous patches and islets of

Tomato+ cells were observed throughout the cornea (Figure 2B). This is in agreement with earlier work indicating that most corneal cells have a neural crest cell origin. Fluorescent axons were not observed in the cornea. Second, we used the *Tau-lox-Stop-lox-mGFP-IRES-nls-lacZ* mice (*Tau*^{GFP}) in which Cre-mediated recombination leads to the permanent expression of a myristoylated GFP in axons and of ß-galactosidase (ß-gal) in nuclei (Hippenmeyer et al., 2005), but only in cells expressing the Tau protein, such as neurons and oligodendrocytes (Hippenmeyer et al., 2005; Young et al., 2013). Confocal imaging of whole-mount corneas (n>30) from *Wnt1:cre;Tau*^{GFP} mice revealed a dense meshwork of GFP-positive axons (Figure 2C) including large axonal bundles in the stroma, typical axonal leashes oriented in a centripetal direction and fine intraepithelial branches (Figure 2D). We also observed an almost perfect overlap between the GFP fluorescence and the ß-III tubulin immunolabeling (n=3), suggesting that the vast majority of corneal nerves were labelled in *Wnt1:cre;Tau*^{GFP} mice. This conclusion was further supported by the analysis of trigeminal ganglia sections in which neuronal nuclei (visualized with Dapi) also expressed ß-gal (Figure 2F). We also used another reporter line *Tau-lox-Stop-lox-Syn-GFP-IRES-nls-lacZpA* mice (*Tau*$^{Syn\text{-}GFP}$) (Pecho-Vrieseling et al., 2009), in which Cre-recombination result in the expression at presynaptic terminals of a fusion protein between the synaptic vesicle protein Synaptophysin and GFP (Figure 2G). As in *Wnt1:cre;Tau*^{GFP} mice, a strong GFP expression was detected in the corneal nerves of *Wnt1:cre;Tau*$^{Syn\text{-}GFP}$ mice (Figure 2H, I). The concentration of the GFP at vesicular release sites (or varicosities) resulted in a beaded-appearance of the GFP signal in the subepithelial plexus and the epithelium (n=10).

These results show that the combination of *Wnt1:cre* and *Tau*^{GFP} and *Tau*$^{Syn\text{-}GFP}$ lines probably allows visualization of the entire population of corneal nerves, most likely including autonomic axons which also belong to the *Wnt1*/neural crest cell lineage (Espinosa-Medina et al., 2014).

TAG-1:cre line

TAG-1 (also known as Contactin-2) is a cell-adhesion molecule of the immunoglobulin superfamily (Furley et al., 1990). TAG-1 is expressed by various types of cells including sensory neurons in the peripheral nervous system, retinal ganglion cells, oligodendrocytes and Schwann cells (Furley et al., 1990; Traka et al., 2002; Chatzopoulou et al., 2008). Therefore, we thought that the recently described *TAG-1:cre* BAC transgenic line (Schmidt et al., 2014) could be used to visualize trigeminal projections (Figure 3A). In *TAG-1:cre;Rosa*^{Tom} mice, a strong Tomato expression was induced in cornea cells (Figure 3B) as observed in the *Wnt1:cre ;Rosa*^{Tom} mice. However, at P0, Tomato expression in *TAG-1:cre;Rosa*^{Tom} was restricted to a few cells in the periphery of the cornea (Data not shown). This suggests that TAG-1 expression in the neural crest cell progeny is not limited to Schwann cells but extend to the cornea. To bypass this problem, we again relied on the *Tau*^{GFP} line and found that most corneal axons, strongly expressed GFP in *TAG-1:cre;Tau*^{GFP} line (Figure 3C-D; n>30) as confirmed by their co-expression of ßIII-tubulin (Figure 3E; n=3). In trigeminal ganglion sections (n=3) from *TAG-1:cre;Tau*^{GFP} mice, ßgal and GFP were co-expressed (Figure 3F) and found in both Neurofilament 200-positive myelinated non-nociceptive axons and Neurofilament 200-negative nociceptive axons (Namavari et al., 2011). The presence of Neurofilament 200+ axons in the mouse cornea has already been reported (Chucair-Elliott et al., 2015).

En1:Cre line

We next continued to test other Cre lines that, unlike the *Wnt1:cre* and *Tag-1:cre* lines, could drive transgene expression in a small subset of trigeminal neurons and therefore result in a sparse labelling of corneal axons.

The *engrailed-1* (*En1*) transcription factor controls the development of some neural crest cell derivatives including the trigeminal placode (Zhong et al., 2010; Deckelbaum et al., 2012). Therefore, we crossed, *En1:cre* mice (Kimmel et al., 2000) with Rosa^{Tom} (n=2) and Tau^{GFP} (n=3) lines (Figure 3H). The results were similar to the two other Cre lines: strong expression of Tomato in cornea cells (Figure 3I) and strong GFP expression in corneal nerves (Figure 3J, K). In the trigeminal ganglia, almost all neurons were GFP+ (Figure 3L) as shown by ßIII-tubulin immunostaining (n=3), and they comprised non-peptidergic (binding IB4; Figure 3L) and peptidergic (CGRP+; Figure 3M) C-fibers.

Islet1 line

Next, we tested the *Islet1:cre* line (Figure 4A) as in mice, this transcription factor controls the formation of the trigeminal ganglia and autonomic ganglia (Sun et al., 2008; Coppola et al., 2010). Islet1 appears to be expressed most if not all trigeminal neurons (Sun et al., 2008; Coppola et al., 2010; Meng et al., 2011). Interestingly, all corneal nerves were found to highly express Tomato in *Islet1:cre;Rosa*^{Tom} corneas (Figure 4B, n>10) as supported by anti-ßIII-Tubulin immunostaining (Figure 4C). This was also the case in the trigeminal ganglia where all CGRP+ and ßIII-Tubulin neurons appeared to express Tomato (n=3) (Figure 4D, E). Therefore, this genetic combination drives the expression of a red fluorescent protein in most, if not all, corneal nerves suggesting that the corresponding neurons either derive from Islet1+ neural crest and placode progenitors or express islet1 when their fate is established. This observation lead us to combine the *CGRP:GFP* and *Islet1:cre;Rosa*^{Tom} lines (Figure 4F). Strikingly, in the compound line, two populations of corneal axons, co-expressing GFP and Tomato or only expressing Tomato, could be visualized by confocal microscopy (n=5) (Figure 4H, I).

Ret:cre^{ER} line

Although all the above lines will be extremely useful to study corneal innervation, they do not reveal the morphology and branching pattern of individual trigeminal axons. To address this problem, we tested the *Ret:cre^{ER}* knockin line (Luo et al., 2009). The Ret receptor tyrosine kinase controls the development of mechanoreceptor neurons (Luo et al., 2009) and is broadly expressed in trigeminal neurons (Coppola et al., 2010) and Ret neurons can be divided into two main groups (Luo et al., 2009). Most Ret+ neurons are peptidergic nociceptors (CGRP+) and a few part are non peptidergic nociceptors. Among this two populations of Ret+ neurons, some have large diameter soma and exhibit features of mechanosensory neurons.

As tamoxifen injection is needed to activate Cre-dependent recombination, it should, in principle, allow temporal control of Cre recombinase activity and modulation of the number of trigeminal neurons activating Cre, by adjusting the dose of tamoxifen injected to the mice.

To test this hypothesis, *Ret:cre^{ER}* mice were first crossed to *Tau^{GFP}* mice (Figure 5A). In absence of tamoxifen, corneas did not contain any fluorescent axons (Figure 5B; n>10). Mice were next injected once with increasing doses of tamoxifen and corneas collected 14 or 60 days later. At the lowest dose (0.25 mg; n>10) a sparse labeling was obtained with only a few GFP+ axons seen in the cornea (Figure 5C). At an intermediate dose (0.5 mg; n=5) the density of GFP+ axons was significantly increased (Figure 5D) but did not fill homogeneously the cornea. When the tamoxifen dose was doubled (1 mg; n>10), the density of fluorescent axons was further increased but still only represented a fraction of the corneal nerves as demonstrated by ßIII-tubulin immunostaining (Figure 5E, F). Next we analyzed *Ret:cre^{ER};Rosa^{Tom}* double transgenic mice. At the lowest tamoxifen dose, the cornea was almost completely filled with Tomato positive cells but a few axons could be imaged despite the high Tomato expression in corneal cells (Figure 5G; n=5). By contrast, at the higher doses, Tomato+ axons were readily seen in addition to corneal cells (Figure 5H, I; n>10). We

next attempted to combine the three lines to determine if combinatorial expression of GFP and Tomato could be achieved when the two reporter lines were simultaneously intercrossed wit the *Ret:cre^{ER}* line. We also used a higher dose of tamoxifen (3 mg) and also immunostained the corneas of *Ret:cre^{ER};Rosa^{Tom};Tau^{GFP}* mice with anti-ßIII tubulin (n=3). This strategy resulted in the multicolor labeling of corneal innervation, with a majority of axons expressing both fluorescent proteins (and therefore appearing yellow) and a lower number of axons expressing a single protein, either Tomato or GFP (Figure 6A, B). This could be partially due to the weaker intensity of the GFP signal. Tomato+ and GFP+ axons (alone or in combination) represented 59% of ßIII tubulin+ axons (n=3).

A similar result was obtained with *Ret:cre^{ER};Rosa^{Tom};Tau$^{Syn\text{-}FP}$* mice (n=3) (Figure 6C, D).

We next crossed the *Ret:cre^{ER};Rosa^{Tom}* and the *CGRP:GFP* lines. The resulting *Ret:cre^{ER};Rosa^{Tom};CGRP:GFP* mice were first injected with a low dose of tamoxifen (n=3). The trajectories of individual Tomato+ axons within larger GFP+ axonal trunks could be followed (Figure 6F) and their terminal arbors as they stem from these large trunks were also visible (Figure 6G). At a high dose of tamoxifen (n=3), GFP and Tomato were expressed in a combinatorial manner in *Ret:cre^{ER};Rosa^{Tom};CGRP:GFP* corneas, with only a small subset of axons expressing only one protein (Figure 6H). Administration of tamoxifen (3mg) to the *Ret:cre^{ER};Rosa^{Tom};CGRP:GFP* reporter adult mice lead to expression of Tomato (D14) in large soma NF200+ neurons, CGRP+ neurons and IB4+ neurons (n=5).

We also used the *Ret:cre^{ER}* mice crossed to *Tau^{GFP}* mice injected with a low dose of tamoxifen (0.25mg) to visualize the morphology and branching pattern of individual corneal axons. Corneal axons of 10 corneas (143 axons in total) were traced using the Imaris Neurofilament tool software on confocal images at a 40x magnification (Figure 7A, B). This showed that individual axons extended relatively straight in a centripetal manner and only bear a few side branches laterally. Reconstructions of superficial nerve terminals in the mouse

corneal epithelium led us to identify 3 types of nerve terminals, as described previously (Ivanusic et al., 2013; Alamri et al., 2015, 2018) simple (Figure 7E, G), 33 multiple (Figure 7C, D, H) and 34 complex (Figure 7F, I). Simple terminals (Figure 7E, G) do not branch after leaving the sub-basal nerves and end with a single, bulbar swelling at the superficial surface of the epithelium. These were more frequent in the center of the cornea than in the periphery. Multiple terminals (Figure 7C, D, H) branch within the epithelium into a small number (usually 3–4) of horizontal fibers that run parallel to the surface. Each of these branches end in a single bulbar swelling similar to those associated with simple terminals. These ramifying terminals were most obvious in the peripheral cornea. The axons forming the complex terminals (Figure 7F, I) form a cluster of highly branched fibers that have many branches. These complex terminals have multiple bulbar endings, and many of these bulbar endings are larger than those associated with the simple and ramifying terminals. Complex terminals were found in both the central and peripheral parts of the cornea. Atlhough a recent study conducted in guinea pig (Alamri et al., 2015), reported morphological differences between localization of axonal endings in terms of basal versus apical epithelium, we were unable to define nerves endings on the basis of their localization in mice.

Other mouse lines tested

Previous studies have identified other transgenic lines in which fluorescent proteins selectively label subsets of axons innervating the hairy skin (Figure 8; see methods for line descriptions). For instance, GFP is expressed by lanceolate Aδ-LTMRs in *TrkB:TauGFP* mice, (Li et al., 2011; Rutlin et al., 2014) and Aß rapidly adapting (RA)-LTMRs in *Split:cre* mice (Rutlin et al., 2014) Aß RA-LTMRs also express tdTomato in *Npy2r :tdTomato* mice (Gong et al., 2003; Li et al., 2011).These two types of LTMRs are absent from the cornea and

accordingly, no fluorescent axons were detectable in corneas from mice belonging to these three lines (Figure 8A-C, n= 2 for each). Scattered GFP-positive cells, possibly resident macrophages (Brissette-storkus et al., 2002), were observed in *TrkB:TauGFP* corneas. Likewise, no GFP-fluorescent nerves were found in the corneas of *Mrgprd:GFP* mice (Figure 8D, n=2) in which GFP is exclusively expressed in non-peptidergic neurons that innervate the epidermis (Zylka et al., 2005). More surprisingly, we could not observe fluorescent axons, in corneas from *VGluT3:GFP* BAC transgenics (Figure 8E) although in the epidermis (n=2), GFP was shown to be expressed in non-peptidergic LTMR-C fibers (Seal et al., 2009) which exist in the cornea (Müller et al., 2003; Alamri et al., 2015).

It was previously shown that YFP is expressed in a large fraction of corneal nerves in *Thy1:YFP* mice (Yu and Rosenblatt, 2007; Namavari et al., 2011; Taylor-Clark et al., 2015). Interestingly, lines expressing a Brainbow cassette under the Thy1 promoter were generated (Livet et al., 2007) suggesting that multicolor labeling of corneal axons could be achieved using the Brainbow strategy. Brainbow is a transgenic system based on Cre-*lox* recombination for stochastic expression of multiple genes coding spectrally distinct fluorescent proteins. We used the *Thy1-Brainbow1.0* line in which the red fluorescent protein tdimer2 (RFP) is expressed by default (Livet et al., 2007), whereas either the blue fluorescent protein mCerulean (CFP) or the yellow fluorescent protein (YFP) are expressed upon Cre-driven recombination. Accordingly, RFP+ axons could be observed in the cornea of *Thy1.Brainbow1.0* mice (data not shown). To trigger the recombination of the Brainbow cassette in corneal nerves we used the *CAG:cre*^{ERT2} line (Guo et al., 2002) that expresses almost ubiquitously a tamoxifen-inducible Cre recombinase. As expected, upon tamoxifen injection (see methods), we could observe axons expressing YFP, CFP or both (Figure 8F), but fluorescence intensity was very low and we could not detect any RFP signal, suggesting

that all cassettes were recombined with the tested protocol (n=3). Therefore, this line was not used further.

Analysis of corneal nerve reorganization during aging.

Our next objective was to use transgenic lines to study the remodeling of corneal nerves during aging as little information on this process is currently available. We focused on the *CGRP:GFP* line as GFP expression is very robust in a well characterized population of corneal axons (peptidergic nociceptors). In *CGRP:GFP* newborns (Figure 9A; n=5), GFP+ axons already formed a dense ring-like network at the periphery of the cornea in the limbal region. GFP+ axons were also found extending towards the center of the cornea but they expressed lower level of GFP (see also Figure 1H). By P10, GFP+ axons covered completely the cornea and terminal intraepithelial branches were numerous but there was not yet any obvious polarization or corneal axons (Figure 9B; n=8). By P21, the typical axonal leashes started to form and to acquire their centripetal orientation (Figure 9C; n=5). This remodeling was more advanced at one month with also the first evidence for the development of an axonal spiral or whorl-like vortex at the center of the cornea (Figure 9D; n=5). In 4 month-old *CGRP:GFP* mice, the corneal innervation pattern of GFP+ axons was fully mature with a clear centripetal polarity and pronounced central vortex (Figure 9E; n=5). Interestingly, between 6-9 month of age (n=10), evidence for a deterioration of the corneal innervation were detected primarily affecting axons located at the cornea apex (Figure 9F, G). The structure of the vortex was often disorganized with either axons lacking a spiral organization or with a disappearance of GFP+ axons in the central region. This was accompanied at older ages (12-18 months; n=6 and 6) by a reduction in the density of CGRP+ axonal leashes followed by the reappearance of disoriented axonal branches seen at immature stages (Figure 9H, I).

Corneal CGRP+ innervation density decreases significantly in the center and in the periphery with the age of the mice at 4 month- (n=5), 12 month- (n=5) and 18 month- (n=5) old. Density in the center of the cornea was measured at 214019 ± 10107 pixels at 4 months and then decreased to 148333 ± 25482 pixels at 12 months (p=0.04) and to 77068 ± 11268 pixels at 18 months (p=0.006). Density in the periphery of the cornea was measured at 173045 ± 12823 pixels at 4 months and then decreased to 80500 ± 8045 pixels at 12 months (p=0.007) and to 55807 ± 7830 pixels at 18 months (p=0.03).

Neuropilin-1 control the postnatal development of the corneal innervation

The molecular factors controlling the development and maintenance of corneal innervation are still largely unknown. Sema3A and Sema3F and their respective receptors, neuropilin-1 and neuropilin-2, control the initial branching of trigeminal axons on the embryonic cornea (McKenna et al., 2012). The embryonic or perinatal lethality of most mice deficient in axon guidance molecules has hampered the analysis of the molecular mechanisms involved in the postnatal development of corneal axons. Interestingly, our genetic screen uncovered several lines expressing Cre recombinase in ophthalmic trigeminal axons. Therefore, we next attempted to use these lines to study the role of axon guidance molecules in the development of cornea innervation.

We first focused on Neuropilin-1 (Npn1), which is the binding component of the receptor complex for Sema3A, a secreted semaphorin expressed in the developing lens and cornea (Lwigale and Bronner-Fraser, 2007; Ko et al., 2010). There is a severe defasciculation of embryonic trigeminal axons in a mouse ENU-mutant expressing a mutated Sema3 unable to bind Neuropilin-1 (Merte et al., 2010) as well as in Sema3A knockout embryos (Ulupinar et al., 1999). To inactivate neuropilin-1 in trigeminal axons, we crossed *Npn1*^{lox} conditional knockouts (Gu et al., 2003) to *TAG-1:cre* mice. To validate this strategy we first studied

trigeminal projections in E12.5 *TAG-1:cre;Npn1^{lox}* embryos, as severe sensory nerve branching defects were previously observed at this age in *Npn1$^{-/-}$* null embryos (Kitsukawa et al., 1997). The ophthalmic branches of the trigeminal nerve were visualized using anti-TAG-1 immunostaining, 3DISCO tissue clearing and 3D light sheet microscopy (Belle et al., 2014). We found that ophthalmic axons were highly defasciculated in *TAG-1:cre;Npn1$^{lox/lox}$* embryos compared to *TAG-1:cre;Npn1$^{lox/+}$* controls (Figure 10A, B; n=3 for each genotype) and the total length of the ophthalmic V1 branch (main trunk and all branches of the superior ophthalmic division of the trigeminal nerve surrounding the eye) was strongly increased (18 ± 1.5 mm in mutant compared to 4.3 ± 0.24 mm in control ; p=0.003); At this age, the cornea of the *TAG-1:cre;Npn1$^{lox/lox}$* embryos was prematurely innervated (Figure 10C, D) containing 1.7 ± 0.11 mm of Tag-1+ axons compared to 0.12 ± 0.03 mm in corneas from controls (p=0.001). A premature innervation of the cornea has been previously reported in embryo from a Neuropilin-1 mutant line in which this receptor is unable to bind its ligand Sema3A (McKenna et al., 2012). These results show that, in this line Neuropilin-1 was inactivated in trigeminal projections to the cornea. In contrast to *Npn1$^{-/-}$* mutants, *TAG-1:cre;Npn1$^{lox/lox}$* mice were viable and survive to adulthood. To visualize trigeminal axons postnatally in conditional knockouts, we crossed them to *Tau^{GFP}* mice.

At birth, abnormal development of corneal innervation was observed in *TAG-1:cre;Npn1$^{lox/lox}$* on confocal images of whole-mount corneas (Figure 10E-H). In comparison with *TAG-1:cre;Npn1$^{lox/+}$* controls (n=3), the density and branching of GFP+ axons was strongly increased in *TAG-1:cre;Npn1$^{lox/lox}$* newborn mice (n=3), both in the subepithelial plexus (98 333 ± 12 583 pixels in mutant versus 34 667 ± 4509 pixels in controls ; p=0.009) and in the stroma (88667 ± 10 969 pixels in mutants versus 17667 ± 2516 pixels in controls; p=0.003). Larger axonal trunks were found in the stroma and more GFP+ axons in the plexus (Figure 10E, G). The abnormal density of GFP+ axons was clearly visible after reslicing of the

images. These obvious and severe branching defects were still seen at P14 (n=3) both in the epithelial plexus (156667 ± 20 816 pixels vs. 93333 ± 10 408 pixels; p=0.03) and in the stroma (128667 ± 18 583 pixels versus 41667 ± 4725 pixels ; p=0.008) and in two-month old adult *TAG-1:cre;Npn1*$^{lox/lox}$ mice (n=6; 320000 ± 26 457 pixels vs. 148333 ± 12583 pixels in the epithelial plexus ; p=0.002 ; 202667 ± 16623 pixels vs. 59667 ± 5507 pixels in the stroma ; p=0.003 ; Figure 10I-L). The presence of Tomato+ cells in the cornea of *TAG-1:cre;Rosa*^{Tom} (Figure 3B) suggests that the axon branching defects observed in the cornea of *TAG-1:cre;Npn1*$^{lox/lox}$ mice could be at least to some extent attributed to abnormal cornea structure although trigeminal axon branching defects are already observed before birth, when only a few Tomato+ cells are present in *TAG-1:cre;Rosa*^{Tom} mice (data not shown). To assess cornea cytoarchitecture, we used DAPI (see methods) and quantified the number of superficial epithelial cells, basal epithelial cells, keratocytes (the only cells present in the stroma) and corneal thickness (n=3 corneas for each genotype; Mann-Withney test) in control and *TAG-1:cre;Npn1*$^{lox/lox}$ mutants. The mean superficial epithelial cells density per µm^2 was 647 ± 69 in mutants *vs* 625 ± 60 cells in controls (p=0.85). The mean basal epithelial cells density per µm^2 was 1607 ± 147 *vs* 1668 ± 113 cells (p=0.78) in mutants and controls respectively. The mean keratocytes density was 182 ± 26 *vs* 165 ± 34 cells / µm^2 (p=0.87) in mutant and control respectively and, the mean corneal thickness was 87 ±10 µm in mutants vs 92 ± 11 µm in controls (p=0.91). Together, these results show that neuropilin-1 is a key regulator of trigeminal axon branching in the cornea.

Discussion

Our knowledge of the organization, ontogenesis and remodeling of corneal innervation has primarily relied on immunolabeling methods. Here, we have tested 22 transgenic lines for their ability to induce the expression of one or multiple fluorescent proteins in corneal axons. We have identified 7 lines, including one BAC transgenic and 6 cre-recombinase driver lines,

555 that efficiently label all or subsets of corneal axons. We further show that a combinatorial and
556 dual expression of more than one fluorescent protein is possible by generating compound
557 transgenic mice. Importantly, this genetic labeling method alleviates the problem of antibody
558 penetration.

559 In the known "cornea nerve mouse lines", *Trpm8:GFP* and *Thy1:YFP* (Yu and Rosenblatt,
560 2007; Parra et al., 2010; Knowlton et al., 2013; Taylor-Clark et al., 2015) only a subset of
561 corneal axons express a green fluorescent protein. By contrast, the whole population of
562 corneal axons could be labelled, using several of our cre-driver lines, as demonstrated by the
563 perfect overlap with ßIII-Tubulin immunolabeling. This suggests that in these lines, Cre is not
564 only expressed in trigeminal projections but also probably in autonomic axons. In all cases,
565 the fluorescent signal was high enough to be imaged directly indicating that it should be
566 possible to image corneal axons in vivo and to perform time-lapse study of their development
567 and response to injury. Importantly, we also identified lines that target a fraction of corneal
568 nerves. The *CGRP:GFP* line will be very useful as it labels peptidergic nociceptors which
569 play a pivotal role in cornea pain (Belmonte et al., 2015). The *Ret:cre*^{ER} line is also
570 particularly interesting as at a low tamoxifen dose, a sparse labeling of a few corneal axons
571 can be achieved. This is unique and will allow to image and reconstruct the arborization and
572 branching pattern of single corneal axons and determine how it develops and respond to
573 injury, inflammation and other pathological conditions. Moreover the morphology of nerve
574 terminals we observed is consistent with a previous description of human corneal innervation
575 (Marfurt et al., 2010), which reported terminals with single endings or more complex tree-like
576 morphologies in the epithelium. Thus, the morphological heterogeneity we found in mice may
577 also be present in humans.
578 Previous studies have suggested that although corneal axons do not establish synaptic contacts
579 in the cornea, they could release neuropeptides such as CGRP and substance P via vesicles

ressembling synaptic vesicles and expressing typical synaptic proteins (Kruger et al., 2003; Talbot and Kubilus, 2018). The presence of GFP+ puncta in corneal axons of *Wnt1cre;Tau^{SynGFP}* mice support these findings. However, it could also just represents a diffusion of the vesicles containing the GFP fusion protein in the peripheral branch of trigeminal axons.

A deeper characterization of these new cornea nerve lines, will require assessing their electrophysiological properties. For instance, it will be important to determine if Aδ fibers are labelled in these lines and if their morphology differs from the C-fibers. Other lines that could also label corneal axons should also be studied such as the *Piezo2:GFP* mice (Woo et al., 2015) and the *TRPV1:cre line* (Cavanaugh et al., 2011). Previous studies reported how mouse corneal nerve terminal density and number change during development (Wang et al., 2012; Reichard et al., 2016). More recently, a study shows the morphological and functional characteristics of corneal TRPM8-EYFP axons and how terminals appeared markedly altered in aged mice (Alcalde et al., 2018). Our study focuses on peptidergic CGRP+ axons and shows anatomic evidence for a significant decrease in corneal peptidergic nerve terminal density as a function of age in the mouse.

The morphological and functional modifications of corneal sensitive innervation with age are part of the general, senescence-induced degenerative processes affecting primary sensory neurons, associated with DNA damage and oxidative stress (Long et al., 2014). These changes are likely reflected in morphometric, ultrastructural and functional alterations of peripheral axons that, in the case of peripheral corneal nerves, may be accelerated by the slowdown in regeneration and remodeling of the nerve terminals that are needed to maintain the innervation of the rapidly turning over surface layers of the corneal epithelium (Alcalde et al., 2018). Interestingly, similar features were described in humans and data from confocal microscopy demonstrated that corneal nerves (particularly sub-basal nerve density) exhibit

pronounced reduction of corneal epithelial nerve terminals and sub-basal nerve fiber density with age (Niederer et al., 2007; He et al., 2010). Increased subbasal nerve tortuosity has also been observed with age (Patel and McGhee, 2009).

An alternative measure of age-related corneal nerve changes is testing the functionality of corneal nerves. Using a Cochet-Bonnet aesthesiometer to test Aδ fiber mechanical sensitivity, corneal sensitivity seems to decrease gradually with age, beginning in the periphery and progressing centrally (Murphy et al., 2004; Roszkowska et al., 2004). Using the Belmonte non-contact aesthesiometer, which measures mechanical stimulation to Aδ fibers and C fibers as well as thermo- and chemoreceptor sensitivity in C fibers, corneal sensitivity begins to decline in the second decade in patients, with major changes (presumably those registered by the Cochet-Bonnet aesthesiometer) becoming apparent by age 50 (Murphy et al., 2004). A reduction of the number and probably functional activity of peptidergic CGRP+ axons probably contribute to dry eye desease observed in aged patients and to the development of accompanying unpleasant dryness sensations.

Previous studies have shown that chemorepulsive axon guidance cue semaphorin 3A (Sema3A) and it receptors neuropilin-1 and plexin-A4 controls the embryonic development of trigeminal axons (Yaron et al., 2005; Lwigale and Bronner-Fraser, 2007; Ko et al., 2010; McKenna et al., 2012). Sema3A, which is expressed in the developing cornea and lens, is thought to control the time-course of cornea invasion by trigeminal axons. Interestingly, adult corneal axons are still responsive to Sema3A repulsive activity (Tanelian et al., 1997; Zhang et al., 2018). However, the postnatal development and adult patterning of corneal nerves in absence of Sema3A signaling has not been studied. Here we confirm that trigeminal axons prematurely invade the cornea in both *neuropilin-1* deficient mice as observed in another *Neuropilin-1* mutant line. We also show that during postnatal development the fasciculation and branching of corneal axons are strongly enhanced in both *neuropilin-1* knockouts.

Corneal innervation defects are still present in adult *neuropilin-1* knockouts. As VEGF is able to bind neuropilin-1, it is possible that some of the defects seen in neuropilin-1 knockout are also due to altered VEGF signaling in addition to Sema3A. However, the development of cornea itself does not seem to be affected in the *TAG-1:cre;Npn1*$^{lox/lox}$ which is consistent with other studies that of another *Neuropilin-1* mutant (McKenna et al., 2012) indicating that trigeminal axon branching defects are probably cell-autonomous. These genetic data confirm that Sema3A/neuropilin-1 are interesting drug targets for corneal nerve regeneration (Bannerman et al., 2008; Omoto et al., 2012).

References

Abraira VE, Ginty DD (2013) The sensory neurons of touch. Neuron 79:618–639.

Alamri A, Bron R, Brock J a, Ivanusic JJ (2015) Transient receptor potential cation channel subfamily V member 1 expressing corneal sensory neurons can be subdivided into at least three subpopulations. Front Neuroanat 9:71.

Alamri AS, Wood RJ, Ivanusic JJ, Brock JA (2018) The neurochemistry and morphology of functionally identified corneal polymodal nociceptors and cold thermoreceptors. PLoS One 13:e0195108.

Alcalde I, Íñigo-Portugués A, González-González O, Almaraz L, Artime E, Morenilla-Palao C, Gallar J, Viana F, Merayo-Lloves J, Belmonte C (2018) Morphological and functional changes in TRPM8-expressing corneal cold thermoreceptor neurons during aging and their impact on tearing in mice. J Comp Neurol 520:633–655.

Bai L, Lehnert BP, Liu J, Neubarth NL, Dickendesher TL, Nwe PH, Cassidy C, Woodbury CJ, Ginty DD (2015) Genetic Identification of an Expansive Mechanoreceptor Sensitive

653 to Skin Stroking. Cell 163:1783–1795.

654 Bautista DM, Siemens J, Glazer JM, Tsuruda PR, Basbaum AI, Stucky CL, Jordt S-E, Julius
655 D (2007) The menthol receptor TRPM8 is the principal detector of environmental cold.
656 Nature 448:204–208.

657 Belle M, Godefroy D, Dominici C, Heitz-Marchaland C, Zelina P, Hellal F, Bradke F,
658 Chédotal A (2014) A Simple Method for 3D Analysis of Immunolabeled Axonal Tracts
659 in a Transparent Nervous System. Cell Rep 9:1191–1201.

660 Belmonte C, Acosta MC, Merayo-Lloves J, Gallar J (2015) What Causes Eye Pain? Curr
661 Ophthalmol Rep 3:111–121.

662 Belmonte C, Gallar J, Pozo MA, Rebollo I (1991) Excitation by irritant chemical substances
663 of sensory afferent units in the cat's cornea. J Physiol 437:709–725.

664 Brissette-storkus CS, Reynolds SM, Lepisto AJ, Hendricks RL (2002) Identification of a
665 Novel Macrophage Population in the Normal Mouse Corneal Stroma. Invest Ophthalmol
666 Vis Sci 43:2264–2271.

667 Bron R, Wood RJ, Brock JA, Ivanusic JJ (2014) Piezo2 expression in corneal afferent
668 neurons. J Comp Neurol 522:2967–2979.

669 Canner JP, Linsenmayer TF, Kubilus JK (2015) Developmental Regulation of Trigeminal
670 TRPA1 by the Cornea. Invest Ophthalmol Vis Sci 56:29–36.

671 Caterina MJ, Schumacher M a, Tominaga M, Rosen T a, Levine JD, Julius D (1997) The
672 capsaicin receptor: a heat-activated ion channel in the pain pathway. Nature 389:816–
673 824.

674 Cavanaugh DJ, Chesler AT, Jackson AC, Sigal YM, Yamanaka H, Grant R, O'Donnell D,

675 Nicoll RA, Shah NM, Julius D, Basbaum AI (2011) Trpv1 Reporter Mice Reveal Highly
676 Restricted Brain Distribution and Functional Expression in Arteriolar Smooth Muscle
677 Cells. J Neurosci 31:5067–5077.

678 Chatzopoulou E, Miguez A, Savvaki M, Levasseur G, Muzerelle A, Muriel M-P, Goureau O,
679 Watanabe K, Goutebroze L, Gaspar P, Zalc B, Karagogeos D, Thomas J-L (2008)
680 Structural requirement of TAG-1 for retinal ganglion cell axons and myelin in the mouse
681 optic nerve. J Neurosci 28:7624–7636.

682 Chucair-Elliott AJ, Zheng M, Carr DJJ (2015) Degeneration and Regeneration of Corneal
683 Nerves in Response to HSV-1 Infection. Invest Ophthalmol Vis Sci 56:1097–1107.

684 Coppola E, D'Autreaux F, Rijli FM, Brunet J-F (2010) Ongoing roles of Phox2 homeodomain
685 transcription factors during neuronal differentiation. Development 137:4211–4220.

686 Coste B, Mathur J, Schmidt M, Earley TJ, Ranade S, Petrus MJ, Dubin AE, Patapoutian A
687 (2010) Piezo1 and Piezo2 Are Essential Components of Distinct Mechanically Activated
688 Cation Channels. Science 330:55–60.

689 Danielian PS, Muccino D, Rowitch DH, Michael SK, McMahon AP (1998) Modification of
690 gene activity in mouse embryos in utero by a tamoxifen-inducible form of Cre
691 recombinase. Curr Biol 8:1323-S2.

692 de Castro F, Silos-Santiago I, de Armentia ML, Barbacid M, Belmonte C (1998) Corneal
693 innervation and sensitivity to noxious stimuli in trk A knockout mice. Eur J Neurosci
694 10:146–152.

695 Deckelbaum RA, Holmes G, Zhao Z, Tong C, Basilico C, Loomis CA (2012) Regulation of
696 cranial morphogenesis and cell fate at the neural crest-mesoderm boundary by engrailed
697 1. Development 139:1346–1358.

Ehmke T, Leckelt J, Reichard M, Weiss H, Hovakimyan M, Heisterkamp A, Stachs O, Baltrusch S (2016) In vivo nonlinear imaging of corneal structures with special focus on BALB/c and streptozotocin-diabetic Thy1-YFP mice. Exp Eye Res 146:137–144.

Espinosa-Medina I, Outin E, Picard C a, Chettouh Z, Dymecki S, Consalez GG, Coppola E, Brunet J-F (2014) Neurodevelopment. Parasympathetic ganglia derive from Schwann cell precursors. Science 345:87–90 Available at: http://www.sciencemag.org/cgi/doi/10.1126/science.1253286 [Accessed July 10, 2014].

Esposito MS, Capelli P, Arber S (2014) Brainstem nucleus MdV mediates skilled forelimb motor tasks. Nature 508:351–356.

Evans AL, Gage PJ (2005) Expression of the homeobox gene Pitx2 in neural crest is required for optic stalk and ocular anterior segment development. Hum Mol Genet 14:3347–3359.

Furley AJ, Morton SB, Manalo D, Karagogeos D, Dodd J, Jessell TM (1990) The axonal glycoprotein TAG-1 is an immunoglobulin superfamily member with neurite outgrowth-promoting activity. Cell 61:157–170.

Gage PJ, Rhoades W, Prucka SK, Hjalt T (2005) Fate Maps of Neural Crest and Mesoderm in the Mammalian Eye. Investig Opthalmology Vis Sci 46:4200.

Gong S, Zheng C, Doughty ML, Losos K, Didkovsky N, Schambra UB, Nowak NJ, Joyner A, Leblanc G, Hatten ME, Heintz N (2003) A gene expression atlas of the central nervous system based on bacterial artificial chromosomes. Nature 425:917–925.

González-González O, Bech F, Gallar J, Merayo-Lloves J, Belmonte C (2017) Functional Properties of Sensory Nerve Terminals of the Mouse Cornea. Investig Opthalmology Vis Sci 58:404.

720 Gu C, Rodriguez ER, Reimert D V, Shu T, Fritzsch B, Richards LJ, Kolodkin AL, Ginty DD
721 (2003) Neuropilin-1 conveys semaphorin and VEGF signaling during neural and
722 cardiovascular development. Dev Cell 5:45–57.

723 Guo C, Yang W, Lobe CG (2002) A cre recombinase transgene with mosaic, widespread
724 tamoxifen-inducible action. genesis 32:8–18.

725 He J, Bazan HEP (2016) Neuroanatomy and Neurochemistry of Mouse Cornea. Investig
726 Opthalmology Vis Sci 57:664.

727 He J, Bazan NG, Bazan HEP (2010) Mapping the entire human corneal nerve architecture.
728 Exp Eye Res 91:513–523.

729 Hippenmeyer S, Vrieseling E, Sigrist M, Portmann T, Laengle C, Ladle DR, Arber S (2005)
730 A Developmental Switch in the Response of DRG Neurons to ETS Transcription Factor
731 Signaling. PLoS Biol 3:e159.

732 Ivanusic JJ, Wood RJ, Brock JA (2013) Sensory and sympathetic innervation of the mouse
733 and guinea pig corneal epithelium. J Comp Neurol 521:877–893.

734 Jones MA, Marfurt CF (1991) Calcitonin gene-related peptide and corneal innervation: A
735 developmental study in the rat. J Comp Neurol 313:132–150.

736 Kimmel RA, Turnbull DH, Blanquet V, Wurst W, Loomis C a., Joyner AL (2000) Two
737 lineage boundaries coordinate vertebrate apical ectodermal ridge formation. Genes Dev
738 14:1377–1389.

739 Kitsukawa T, Shimizu M, Sanbo M, Hirata T, Taniguchi M, Bekku Y, Yagi T, Fujisawa H
740 (1997) Neuropilin-semaphorin III/D-mediated chemorepulsive signals play a crucial role
741 in peripheral nerve projection in mice. Neuron 19:995–1005.

742 Knowlton WM, Palkar R, Lippoldt EK, McCoy DD, Baluch F, Chen J, McKemy DD (2013)
743 A Sensory-Labeled Line for Cold: TRPM8-Expressing Sensory Neurons Define the
744 Cellular Basis for Cold, Cold Pain, and Cooling-Mediated Analgesia. J Neurosci
745 33:2837–2848.

746 Ko J-A, Mizuno Y, Yanai R, Chikama T, Sonoda K-H (2010) Expression of semaphorin 3A
747 and its receptors during mouse corneal development. Biochem Biophys Res Commun
748 403:305–309.

749 Kruger L, Light AR, Schweizer FE (2003) Axonal terminals of sensory neurons and their
750 morphological diversity. J Neurocytol 32:205–216.

751 Le Pichon CE, Chesler AT (2014) The functional and anatomical dissection of somatosensory
752 subpopulations using mouse genetics. Front Neuroanat 8:21.

753 Lele P., Weddell G (1959) Sensory nerves of the cornea and cutaneous sensibility. Exp
754 Neurol 1:334–359.

755 Li L, Rutlin M, Abraira VE, Cassidy C, Kus L, Gong S, Jankowski MP, Luo W, Heintz N,
756 Koerber HR, Woodbury CJ, Ginty DD (2011) The Functional Organization of Cutaneous
757 Low-Threshold Mechanosensory Neurons. Cell 147:1615–1627.

758 Livet J, Weissman T a, Kang H, Draft RW, Lu J, Bennis R a, Sanes JR, Lichtman JW (2007)
759 Transgenic strategies for combinatorial expression of fluorescent proteins in the nervous
760 system. Nature 450:56–62.

761 Long YC, Tan TMC, Takao I, Tang BL (2014) The biochemistry and cell biology of aging:
762 metabolic regulation through mitochondrial signaling. Am J Physiol Endocrinol Metab
763 306:E581-91.

764 Luo W, Enomoto H, Rice FL, Milbrandt J, Ginty DD (2009) Molecular Identification of
765 Rapidly Adapting Mechanoreceptors and Their Developmental Dependence on Ret
766 Signaling. Neuron 64:841–856.

767 Lwigale PY, Bronner-Fraser M (2007) Lens-derived Semaphorin3A regulates sensory
768 innervation of the cornea. Dev Biol 306:750–759.

769 Madisen L, Zwingman TA, Sunkin SM, Oh SW, Zariwala HA, Gu H, Ng LL, Palmiter RD,
770 Hawrylycz MJ, Jones AR, Lein ES, Zeng H (2010) A robust and high-throughput Cre
771 reporting and characterization system for the whole mouse brain. Nat Neurosci 13:133–
772 140.

773 Marfurt CF (1988) Sympathetic innervation of the rat cornea as demonstrated by the
774 retrograde and anterograde transport of horseradish peroxidase-wheat germ agglutinin. J
775 Comp Neurol 268:147–160.

776 Marfurt CF, Cox J, Deek S, Dvorscak L (2010) Anatomy of the human corneal innervation.
777 Exp Eye Res 90:478–492.

778 Marfurt CF, Ellis LC (1993) Immunohistochemical localization of tyrosine hydroxylase in
779 corneal nerves. J Comp Neurol 336:517–531.

780 Marfurt CF, Kingsley RE, Echtenkamp SE (1989) Sensory and sympathetic innervation of the
781 mammalian cornea. A retrograde tracing study. Invest Ophthalmol Vis Sci 30:461–472.

782 Marfurt CF, Murphy CJ, Florczak JL (2001) Morphology and neurochemistry of canine
783 corneal innervation. Investig Ophthalmol Vis Sci 42:2242–2251.

784 McKenna CC, Munjaal RP, Lwigale PY (2012) Distinct Roles for Neuropilin1 and
785 Neuropilin2 during Mouse Corneal Innervation. PLoS One 7:e37175.

786 Meng H, Yuan Y, Lee VM (2011) Loss of Sphingosine Kinase 1/S1P Signaling Impairs Cell
787 Growth and Survival of Neurons and Progenitor Cells in the Developing Sensory
788 Ganglia Najbauer J, ed. PLoS One 6:e27150.

789 Merte J, Wang Q, Vander Kooi CW, Sarsfield S, Leahy DJ, Kolodkin AL, Ginty DD (2010)
790 A Forward Genetic Screen in Mice Identifies Sema3AK108N, which Binds to
791 Neuropilin-1 but Cannot Signal. J Neurosci 30:5767–5775.

792 Müller LJ, Marfurt CF, Kruse F, Tervo TMT (2003) Corneal nerves: structure, contents and
793 function. Exp Eye Res 76:521–542.

794 Murata Y, Masuko S (2006) Peripheral and central distribution of TRPV1, substance P and
795 CGRP of rat corneal neurons. Brain Res 1085:87–94.

796 Murphy PJ, Patel S, Kong N, Ryder REJ, Marshall J (2004) Noninvasive assessment of
797 corneal sensitivity in young and elderly diabetic and nondiabetic subjects. Invest
798 Ophthalmol Vis Sci 45:1737–1742.

799 Nakamura A, Hayakawa T, Kuwahara S, Maeda S, Tanaka K, Seki M, Mimura O (2007)
800 Morphological and immunohistochemical characterization of the trigeminal ganglion
801 neurons innervating the cornea and upper eyelid of the rat. J Chem Neuroanat 34:95–
802 101.

803 Namavari A, Chaudhary S, Sarkar J, Yco L, Patel K, Han KY, Yue BY, Chang J-H, Jain S
804 (2011) In Vivo Serial Imaging of Regenerating Corneal Nerves after Surgical
805 Transection in Transgenic Thy1-YFP mice. Investig Opthalmology Vis Sci 52:8025.

806 Niederer RL, Perumal D, Sherwin T, McGhee CNJ (2007) Age-related differences in the
807 normal human cornea: a laser scanning in vivo confocal microscopy study. Br J
808 Ophthalmol 91:1165–1169.

809 Omoto M, Yoshida S, Miyashita H, Kawakita T, Yoshida K, Kishino A, Kimura T, Shibata S,
810 Tsubota K, Okano H, Shimmura S (2012) The Semaphorin 3A Inhibitor SM-345431
811 Accelerates Peripheral Nerve Regeneration and Sensitivity in a Murine Corneal
812 Transplantation Model Thurtell M, ed. PLoS One 7:e47716.

813 Parra A, Madrid R, Echevarria D, del Olmo S, Morenilla-Palao C, Acosta MC, Gallar J,
814 Dhaka A, Viana F, Belmonte C (2010) Ocular surface wetness is regulated by TRPM8-
815 dependent cold thermoreceptors of the cornea. Nat Med 16:1396–1399.

816 Patel D V, McGhee CNJ (2009) In vivo confocal microscopy of human corneal nerves in
817 health, in ocular and systemic disease, and following corneal surgery: a review. Br J
818 Ophthalmol 93:853–860.

819 Pecho-Vrieseling E, Sigrist M, Yoshida Y, Jessell TM, Arber S (2009) Specificity of sensory-
820 motor connections encoded by Sema3e-Plxnd1 recognition. Nature 459:842–846.

821 Preibisch S, Saalfeld S, Tomancak P (2009) Globally optimal stitching of tiled 3D
822 microscopic image acquisitions. Bioinformatics 25:1463–1465.

823 Quallo T, Vastani N, Horridge E, Gentry C, Parra A, Moss S, Viana F, Belmonte C,
824 Andersson D a., Bevan S (2015) TRPM8 is a neuronal osmosensor that regulates eye
825 blinking in mice. Nat Commun 6:7150.

826 Ranade SS, Woo S-H, Dubin AE, Moshourab R a., Wetzel C, Petrus M, Mathur J, Bégay V,
827 Coste B, Mainquist J, Wilson a. J, Francisco AG, Reddy K, Qiu Z, Wood JN, Lewin
828 GR, Patapoutian A (2014) Piezo2 is the major transducer of mechanical forces for touch
829 sensation in mice. Nature 516:121–125.

830 Reichard M, Hovakimyan M, Guthoff RF, Stachs O (2014) In vivo visualisation of murine
831 corneal nerve fibre regeneration in response to ciliary neurotrophic factor. Exp Eye Res

120:20–27.

Reichard M, Weiss H, Poletti E, Ruggeri A, Guthoff RF, Stachs O, Baltrusch S (2016) Age-Related Changes in Murine Corneal Nerves. Curr Eye Res 41:1021–1028.

Roszkowska AM, Colosi P, Ferreri FMB, Galasso S (2004) Age-Related Modifications of Corneal Sensitivity. Ophthalmologica 218:350–355.

Rózsa AJ, Beuerman RW (1982) Density and organization of free nerve endings in the corneal epithelium of the rabbit. Pain 14:105–120.

Rutlin M, Ho C-Y, Abraira VE, Cassidy C, Bai L, Woodbury CJ, Ginty DD (2014) The Cellular and Molecular Basis of Direction Selectivity of Aδ-LTMRs. Cell 159:1640–1651.

Schmidt ERE, Brignani S, Adolfs Y, Lemstra S, Demmers J, Vidaki M, Donahoo A-LS, Lilleväli K, Vasar E, Richards LJ, Karagogeos D, Kolk SM, Pasterkamp RJ (2014) Subdomain-Mediated Axon-Axon Signaling and Chemoattraction Cooperate to Regulate Afferent Innervation of the Lateral Habenula. Neuron 83:372–387.

Seal RP, Wang X, Guan Y, Raja SN, Woodbury CJ, Basbaum AI, Edwards RH (2009) Injury-induced mechanical hypersensitivity requires C-low threshold mechanoreceptors. Nature 462:651–655.

Shimizu T, Toriumi H, Sato H, Shibata M, Nagata E, Gotoh K, Suzuki N (2007) Distribution and origin of TRPV1 receptor-containing nerve fibers in the dura mater of rat. Brain Res 1173:84–91.

Steventon B, Mayor R, Streit A (2014) Neural crest and placode interaction during the development of the cranial sensory system. Dev Biol 389:28–38.

854 Sun Y, Dykes IM, Liang X, Eng SR, Evans SM, Turner EE (2008) A central role for Islet1 in
855 sensory neuron development linking sensory and spinal gene regulatory programs. Nat
856 Neurosci 11:1283–1293.

857 Talbot CJ, Kubilus JK (2018) Developmental analysis of SV2 in the embryonic chicken
858 corneal epithelium. Exp Eye Res 172:137–143.

859 Tanelian DL, Barry MA, Johnston SA, Le T, Smith GM (1997) Semaphorin III can repulse
860 and inhibit adult sensory afferents in vivo. Nat Med 3:1398–1401.

861 Taylor-Clark TE, Wu KY, Thompson JA, Yang K, Bahia PK, Ajmo JM (2015) Thy1.2 YFP-
862 16 transgenic mouse labels a subset of large-diameter sensory neurons that lack TRPV1
863 expression. PLoS One 10:1–16.

864 Traka M, Dupree JL, Popko B, Karagogeos D (2002) The neuronal adhesion protein TAG-1 is
865 expressed by Schwann cells and oligodendrocytes and is localized to the juxtaparanodal
866 region of myelinated fibers. J Neurosci 22:3016–3024.

867 Ulupinar E, Datwani A, Behar O, Fujisawa H, Erzurumlu R (1999) Role of Semaphorin III in
868 the Developing Rodent trigeminal system. Mol Cell Neurosci 13:281–292.

869 Wang C, Fu T, Xia C, Li Z (2012) Changes in mouse corneal epithelial innervation with age.
870 Investig Ophthalmol Vis Sci 53:5077–5084.

871 Woo S-H, Lukacs V, de Nooij JC, Zaytseva D, Criddle CR, Francisco A, Jessell TM,
872 Wilkinson KA, Patapoutian A (2015) Piezo2 is the principal mechanotransduction
873 channel for proprioception. Nat Neurosci 18:1756–1762.

874 Yang L, Cai C-L, Lin L, Qyang Y, Chung C, Monteiro RM, Mummery CL, Fishman GI,
875 Cogen A, Evans S (2006) Isl1Cre reveals a common Bmp pathway in heart and limb

development. Development 133:1575–1585.

Yaron A, Huang P-H, Cheng H-J, Tessier-Lavigne M (2005) Differential Requirement for Plexin-A3 and -A4 in Mediating Responses of Sensory and Sympathetic Neurons to Distinct Class 3 Semaphorins. Neuron 45:513–523.

Young KM, Psachoulia K, Tripathi RB, Dunn S-J, Cossell L, Attwell D, Tohyama K, Richardson WD (2013) Oligodendrocyte Dynamics in the Healthy Adult CNS: Evidence for Myelin Remodeling. Neuron 77:873–885.

Yu CQ, Rosenblatt MI (2007) Transgenic corneal neurofluorescence in mice: A new model for in vivo investigation of nerve structure and regeneration. Investig Ophthalmol Vis Sci 48:1535–1542.

Zander E, Weddell G (1951) Observations on the innervation of the cornea. J Anat 85:68–99.

Zhang M, Zhou Q, Luo Y, Nguyen T, Rosenblatt MI, Guaiquil VH (2018) Semaphorin3A induces nerve regeneration in the adult cornea-A switch from its repulsive role in development. PLoS One 13:1–16.

Zhong S, Chen X, Cai Q, Luo X, Chen X, Liu J, Yao Z (2010) Dynamic Expression and Heterogeneous Intracellular Location of En-1 during Late Mouse Embryonic Development. Cells Tissues Organs 191:289–300.

Zimmerman A, Bai L, Ginty DD (2014) The gentle touch receptors of mammalian skin. Science 346:950–955.

Zylka MJ, Rice FL, Anderson DJ (2005) Topographically Distinct Epidermal Nociceptive Circuits Revealed by Axonal Tracers Targeted to Mrgprd. Neuron 45:17–25.

Figure Legends

Figure 1

Visualization of corneal peptidergic axons in CGRP:GFP mice.

All pictures (except D and F) are maximal intensity z-projection confocal stacks from whole-mount corneas.

A, Schematic of the CGRP:GFP BAC transgenic construct. GFP was inserted downstream the promoter of the *Calca* gene which encode CGRP. B-G, Images from adult CGRP:GFP mice. B, Flat mount view of a whole-mount cornea, showing GFP expression in corneal nerves. C, Cornea immuno-labelled with anti-GFP with Dapi counterstaining (blue). There is a perfect overlap (merge) between the endogenous GFP fluorescence (green) and the anti-GFP immunoreactivity (red). D, is a reslice of the cornea (54µm thick optical section) showing the location of the GFP axons in the stroma (st), subbasal plexus (sp) and epithelium (e). E, Cornea immuno-labelled with anti-CGRP (red). All CGRP axons are also GFP+. F, Cryostat section of the trigeminal ganglion stained with IB4 (blue) and immuno-labelled for ßIII-Tubulin (red). GFP neurons only represent a subset of ßIII-Tub+ trigeminal neurons. G, Cornea immuno-labelled with anti-ßIII-Tubulin (red). Typical corneal axon leashes of almost parallel GFP+ axons (green) are seen. GFP is only expressed in a subset of corneal nerves. H, at P0, The endogenous GFP expression is weaker than after anti-GFP immunostaining (magenta). All corneal axons in this domain can be seen with anti-ßIII-Tubulin immunostaining (white, right panel). I, GFP+ axons in the P10 cornea immune-labelled for ßIII-Tubulin.

Figure 2

Visualization of corneal axons in Wnt1:cre mice.

All pictures (except F and I) are maximal intensity z-projection confocal stacks from adult whole-mount corneas.

A, Schematic description of the mouse lines. In *Wnt1:cre* knockin mice, Cre recombinase was placed downstream of the *Wnt1* promoter. $Rosa^{Tom}$: the tdTomato coding sequence was inserted in the *Rosa* locus downstream of a lox-STOP-lox cassette. In Tau^{GFP} mice, a lox-STOP-lox cassette preceding a myristoylated *GFP* sequence, followed by an Internal ribosome entry site (IRES) cDNA and the *lacZ* sequence with a nuclear localization signal (nls) was inserted by homologous recombination in the *Tau* locus. B, Islets of corneal cells express Tomato (red) in *Wnt1:cre;*$Rosa^{Tom}$ mice. C, D, Illustrate the dense network of GFP+ corneal axons in *Wnt1:cre;*Tau^{GFP} mice. The apical vortex is shown in D. The inset shows terminal intra-epithelial branches. E, Cornea immunolabelled with anti-ßIII-Tubulin antibodies (red). GFP and ßIII-Tubulin nicely overlap. F, Cryostat section of the trigeminal ganglion at the level of the ophthalmic V1 division stained Dapi (blue) and immuno-labelled for ß-galactosidase (red). GFP+ trigeminal neurons express ß-gal in their nucleus. G, Description of the mouse lines. *Wnt1:cre*, see above; In $Tau^{Syn\text{-}GFP}$ mice, a lox-STOP-lox cassette preceding a cDNA encoding *Synaptophysin* fused to *GFP*, followed by an Internal ribosome entry site (IRES) cDNA and the *lacZ* sequence with a nuclear localization signal (nls) was inserted by homologous recombination in the *Tau* locus. H, Beaded appearance of the GFP signal in *Wnt1cre;*Tau^{SynGFP} mice. I, is a reslice of the cornea with Dapi counterstaining (blue).

Figure 3

Visualization of corneal axons in TAG-1:cre and En1:cre adult mice.

B-E and I-K are maximal intensity z-projection confocal stacks from adult whole-mount corneas. F-G and L, M are confocal images of cryostat sections of trigeminal ganglia.

A, Description of the mouse lines. *Rosa*^{Tom} and *Tau*^{GFP} see Figure 2; In the *TAG-1-cre* BAC transgenic construct, cre recombinase was inserted downstream the promoter of the *Tag-1/Cntn2* gene in an artificial chromosome. B, Tomato is highly expressed by corneal cells in *TAG-1:cre;Rosa*^{Tom} mice. C, D, Illustrate the dense network of GFP+ corneal axons in *TAG-1:cre;Tau*^{GFP} mice. The apical vortex is shown in D. E, Cornea immunolabelled with anti-ßIII-Tubulin antibodies (red). GFP and ßIII-Tubulin perfectly overlap. F, G, In the trigeminal ganglion, GFP+ neurons express ß-gal in their nucleus (F). All GFP+ neurons are also ßIII-Tubulin+ and some are also NF200+ (G). H, Description of the mouse lines. *Rosa*^{Tom} and *Tau*^{GFP} see Figure 2; In *En1:cre* knockin mice, the first exon of the *engrailed-1* gene was replaced by the *cre* sequence using homologous recombination. I, Tomato is highly expressed by a large fraction of corneal cells in *En1:cre;Rosa*^{Tom} mice. J, K, Illustrate GFP+ corneal axons in *En1:cre;Tau*^{GFP} mice. The apical vortex is shown in K. L, M, In the trigeminal ganglion, all IB4+ and all ßIII-immunoreactive neurons are GFP+ (L). GFP is also expressed in the CGRP+ and NF200+ populations (M).

Figure 4

Visualization of corneal axons in Islet1:cre adult mice.

B, C, G, H are maximal intensity z-projection confocal stacks from adult whole-mount corneas.

A, Description of the mouse lines. *Rosa*^{Tom} see Figure 2; In *Islet1:cre* knockin mice, the coding sequence of *cre* was inserted in the *isl1* gene by homologous recombination. B, C, In *Islet1:cre;Rosa*^{Tom} mice, all corneal axons express Tomato (red). ßIII-Tubulin immunoreactive axons (green) are also Tomato+ (see merge). D, E, Confocal images of cryostat sections of trigeminal ganglia. D, illustrates the colocalization of the GFP signal (green) and ßIII-Tub immunoreactivity (red) in trigeminal neurons. E, all CGRP+ neurons

(Cyan) co-express Tomato. F, Description of the mouse lines. *Islet1:cre*, see above. *CGRP:GFP*, see Figure 1; *Rosa*^{Tom} see Figure 2. G, GFP and Tomato expression in whole-mount cornea from an *Islet1:cre;Rosa*^{Tom}*;CGRP:GFP* mouse. H; high magnification showing that Tomato (red) is expressed both by peptidergic (GFP+, Green) and non-peptidergic (GFP-) axons. I, is a reslice of the cornea (54 µm thick optical section) showing the location of the fluorescent axons. GFP+/Tomato+ peptidergic nociceptor axons appear in yellow and the non-petidergic in red.

Figure 5

Visualization of corneal axons in Ret:cre^{ER} adult mice.

B-I are maximal intensity z-projection confocal stacks from adult whole-mount corneas.

A, Description of the mouse lines. *Rosa*^{Tom} and *Tau*^{GFP} see Figure 2; In *Ret:cre*^{ER} knockin mice, the coding sequence of *cre*^{ERT2} was inserted in the first exon of the *Ret* gene by homologous recombination. B, in absence of tamoxifen, no GFP signal is detected in the cornea of *Ret:cre*^{ER}*;Tau*^{GFP}mice. C-E, The number of GFP+ axons increases with the dose of tamoxifen injected (0.25mg-1mg). Corneas were collected 14 days (D14) or 60 days (D60) after injection. F, Immunostaining for anti-ßIII-Tubulin shows that GFP is only expressed in a fraction of ßIII-Tub+ corneal axons. G-I, are corneas from *Ret:cre*^{ER}*;Rosa*^{Tom} mice injected with increasing doses of tamoxifen injected (0.25mg-3mg). At the lowest dose (G) many Tomato+ corneal cells are seen and mask Tomato+ axons. At higher doses (H, I), highly fluorescent cells are seen in the limbal region (arrowheads), and more Tomato+ axons (arrows) are observed.

Figure 6

Analysis of corneal nerves in Ret:cre^{ER} compound mice.

All images (except B and D) are maximal intensity z-projection confocal stacks from adult whole-mount corneas.

A, Cornea from a *Ret:cre^{ER};Tau^{GFP};Rosa^{Tom}* mouse immunolabelled for ßIII-Tubulin. Some ßIII-Tub+ axons (blue) also co-express GFP and Tomato (and appear white). Other axons that only express GFP (green or cyan on the right panel) or only Tomato (red or magenta on the right panel). B, Is a reslice of the cornea (54µm thick optical section) illustrating the distribution of the fluorescent axons in the stroma and epithelium. C, Image of the apex of the cornea and axonal whorl from a *Ret:cre^{ER};Tau$^{Syn\text{-}GFP}$;Rosa^{Tom}* mouse. The three types of axons are seen: GFP+, Tomato+ and a majority of GFP+/Tomato+ axons. D is a reslice of the cornea (54µm thick optical section). E, Description of the mouse lines. *CGRP:GFP*, see Figure 1; *Rosa^{Tom}* see Figure 2; *Ret:cre^{ER}*, see Figure 5. F, G, with a low dose of tamoxifen (0.25 mg), only a few Tomato+ axons and do not always overlap with GFP+ nociceptive axons. The arrowhead in the middle panel indicates the area seen on the high magnification image of a single tomato+ terminal arbor (right panel). H, With a high dose of tamoxifen, most axons co-express GFP and Tomato, but a few only express a single fluorescent protein.

Figure 7

Heterogenous terminal arborization of corneal axons

A, maximal intensity z-projection confocal stacks from adult *Ret:cre^{ER};Tau^{GFP}* whole-mount corneas injected with a low dose of tamoxifen (0.25 mg). B, Axons from (A) were analyzed with Imaris software using the Filament Tracer module. C, high magnification showing single axons in a saggital view. D, single axon tracing showing ramifying nerve terminal. E, single axon tracing showing simple nerve terminal. F, single axon tracing showing complex nerve terminal. G, H, I are reconstructions of superficial nerve terminals in the mouse corneal

epithelium showing examples of simple (G), ramifying (H) and complex (I) nerve terminals based on 143 axons.

Figure 8

Other transgenic lines tested.

Maximal intensity z-projection confocal stacks (A, F) or epifluorescence images (B-E) from adult whole-mount corneas. A-E, no fluorescent corneal axons were detected in *TrkB:Tau^{GFP}*, *Split:cre:GFP, Npy2r:tdTomato, Mrgprd:GFP* and *Vglut3:GFP* mice. Note the presence of scattered GFP+ cells in *TrkB:Tau^{GFP}* line. F, Cornea from a 12 month-old *CAG:cre^{ERT2};Thy1-Brainbow1.0* mouse injected with 0.3mg of tamoxifen at P0. A few CFP+ axons (blue) and YFP+ (green) axons are seen. The arrowhead in the left and middle panel indicate a CFP+/YFP+ double labelled axons, whereas the arrow show axons that are either YFP+ or CFP+.

Figure 9

Age-dependent evolution of the corneal innervation in CGRP:GFP mice.

All images are maximal intensity z-projection confocal stacks from whole-mount corneas. A negative image was generated as fluorescent axons are more visible in black on a white background. A-D, Developmental time-course of corneal innervation in *CGRP:GFP* mice during the first postnatal month. Note the progressive centripetal extension and polarization of the axonal leashes. See text for details. E, at 4 month the axonal vortex at the center of the cornea is well formed (compare with D). F-H, shows abnormal pattern of innervation in the center of the cornea, frequently observed from 6-9 months. Note also in H, the lower density of GFP+ axons compared to E. I, cornea from an 18-month old *CGRP:GFP* mouse. The axonal whorl is absent and axonal leashes are not seen in the center of the cornea and polarity

is perturbed. Larger areas do not contain GFP+ axons. J-L, are wild type corneas immunolabelled with anti-Tubulin. The progressive thinning of corneal innervation is also seen from 9 months, as well as the disorganization of axonal leashes in a one year old mouse.

Figure 10

Neuropilin-1 controls the development of corneal innervation.

A-D, Light sheet microscopy 3D images of E12.5 *TAG-1:cre;Npn1*$^{lox/+}$ (A, C) and *TAG-1:cre;Npn1*$^{lox/lox}$ (B, D) embryos, immunolabelled with anti-Tag-1 antibodies and cleared with 3DISCO. Tag-1+ sensory axons innervating the face are more numerous and highly defasciculated in *TAG-1:cre;Npn1*$^{lox/lox}$ embryo. Trigeminal axons have already invaded the cornea (arrows) in the mutant unlike in the heterozygous control. E-F, Confocal images of GFP+ axons in the cornea from a *TAG-1:cre;Npn1*$^{lox/+}$*;Tau*^{GFP} newborn mouse at the level of the epithelium (E; Epithel.) or the stroma (E; stromal trunks) and the whole cornea (F). The GFP+ axons already form a dense network in the subbasal plexus (arrowheads). A few large axonal trunks are found in the stroma. The bottom panel is a 54µm reslice through the cornea stack. F, Maximal intensity z-projection confocal stack from a whole-mount *TAG-1:cre;Npn1*$^{lox/+}$*;Tau*^{GFP} cornea. G, H, Confocal images of GFP+ axons in the cornea from a *TAG-1:cre;Npn1*$^{lox/lox}$*;Tau*^{GFP} newborn mouse. The density of GFP+ axons and branches is strongly increased in the subbasal plexus (G, left panel) compared to heterozygous controls. The stroma also contains a much higher number of large axonal trunks (right panel). The bottom panel is a 54µm reslice through the cornea stack. H, Maximal intensity z-projection confocal stack from a whole-mount *TAG-1:cre;Npn1*$^{lox/lox}$*;Tau*^{GFP} cornea. I-L, Illustrate that the density of GFP+ axonal branches and large nerve trunks (arrowheads) in the epithelium and stroma is still abnormally high in *TAG-1:cre;Npn1*$^{lox/lox}$*;Tau*^{GFP} mice at P14 (K) and at 2 months (L) compared to aged matched *TAG-1:cre;Npn1*$^{lox/+}$*;Tau*^{GFP}mice (I, J). Occasional

large accumulations of axons are also seen in the knockout (arrow in L). The bottom panels are 54µm reslices of the confocal image stacks. Dapi counterstaining of adult corneas from *TAG-1:cre;Npn1*$^{lox/+}$*;Tau*^{GFP} (M) *and TAG-1:cre;Npn1*$^{lox/lox}$*;Tau*^{GFP} (N) mice. Density of superficial epithelial cells, basal epithelial cells and keratocytes in the stroma; are similar in mutant and control mice.

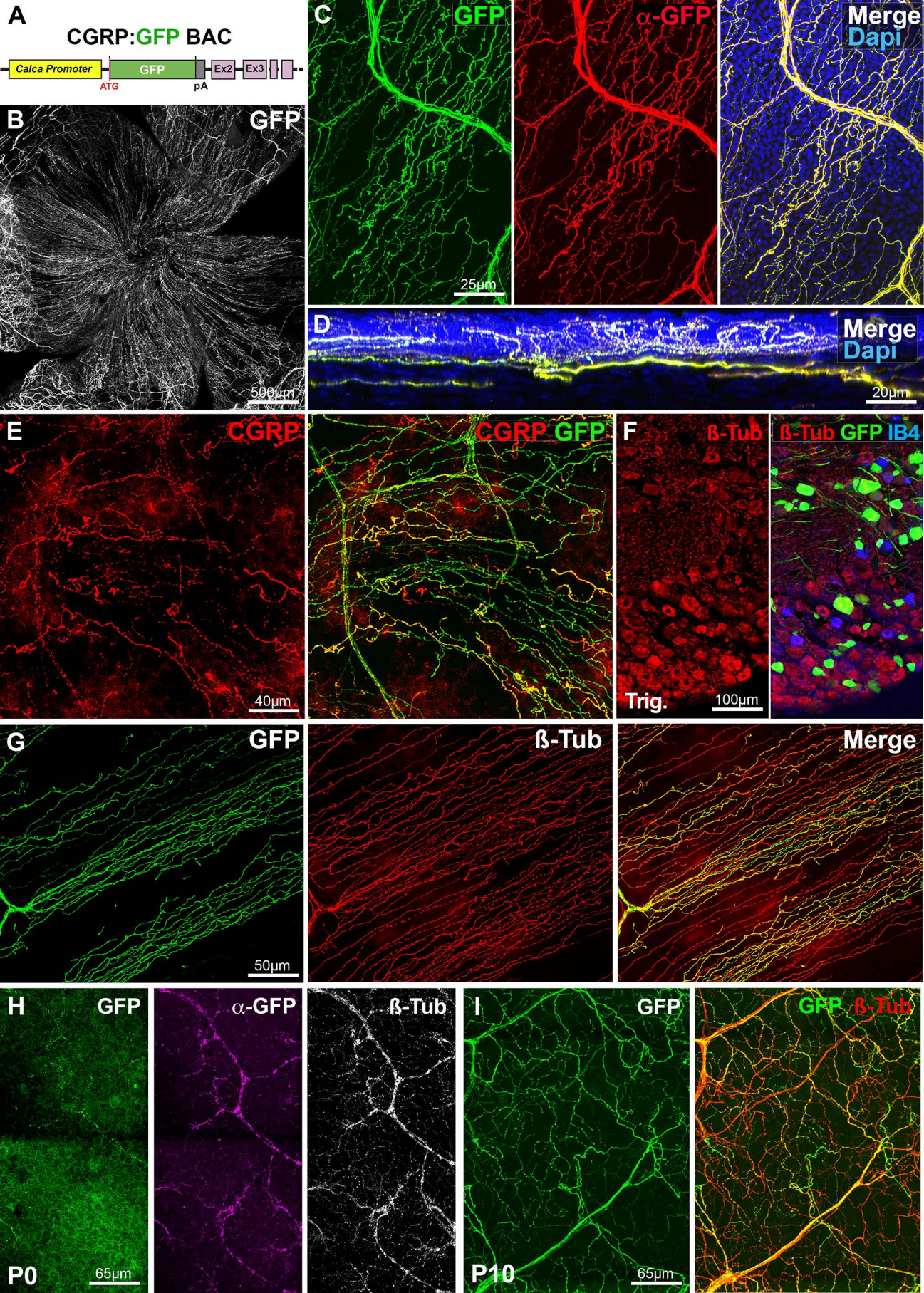
A
CGRP:GFP BAC
Calca Promoter
GFP
Ex2
Ex3
ATG
pA
B
GFP
500µm
C
GFP
α-GFP
Merge
Dapi
25µm
D
Merge
Dapi
20µm
E
CGRP
CGRP GFP
40µm
F
ß-Tub
ß-Tub GFP IB4
Trig.
100µm
G
GFP
ß-Tub
Merge
50µm
H
GFP
α-GFP
ß-Tub
P0
65µm
I
GFP
GFP ß-Tub
P10
65µm

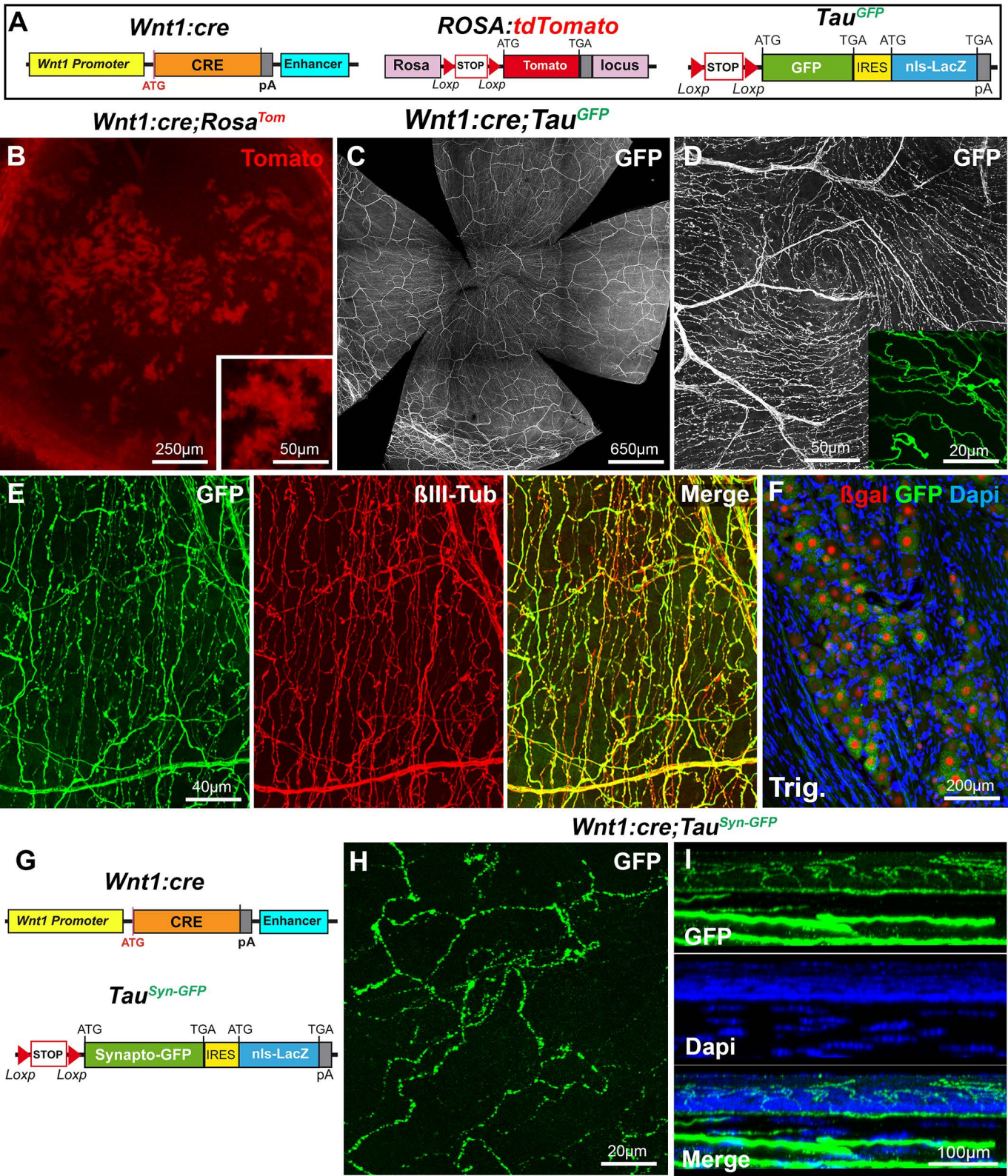
A
Wnt1:cre
Wnt1 Promoter
CRE
Enhancer
ATG
pA
ROSA:tdTomato
Rosa
STOP
Loxp
Loxp
ATG
Tomato
TGA
locus
Tau GFP
ATG
TGA
ATG
TGA
STOP
Loxp
Loxp
GFP
IRES
nls-LacZ
pA
Wnt1:cre;Rosa Tom
Wnt1:cre;Tau GFP
B
Tomato
250µm
50µm
C
GFP
650µm
D
GFP
50µm
20µm
E
GFP
40µm
ßIII-Tub
Merge
F
ßgal GFP Dapi
Trig.
200µm
G
Wnt1:cre
Wnt1 Promoter
CRE
Enhancer
ATG
pA
Tau Syn-GFP
ATG
TGA
ATG
TGA
STOP
Synapto-GFP
IRES
nls-LacZ
Loxp
Loxp
pA
Wnt1:cre;Tau Syn-GFP
H
GFP
20µm
I
GFP
Dapi
Merge
100µm

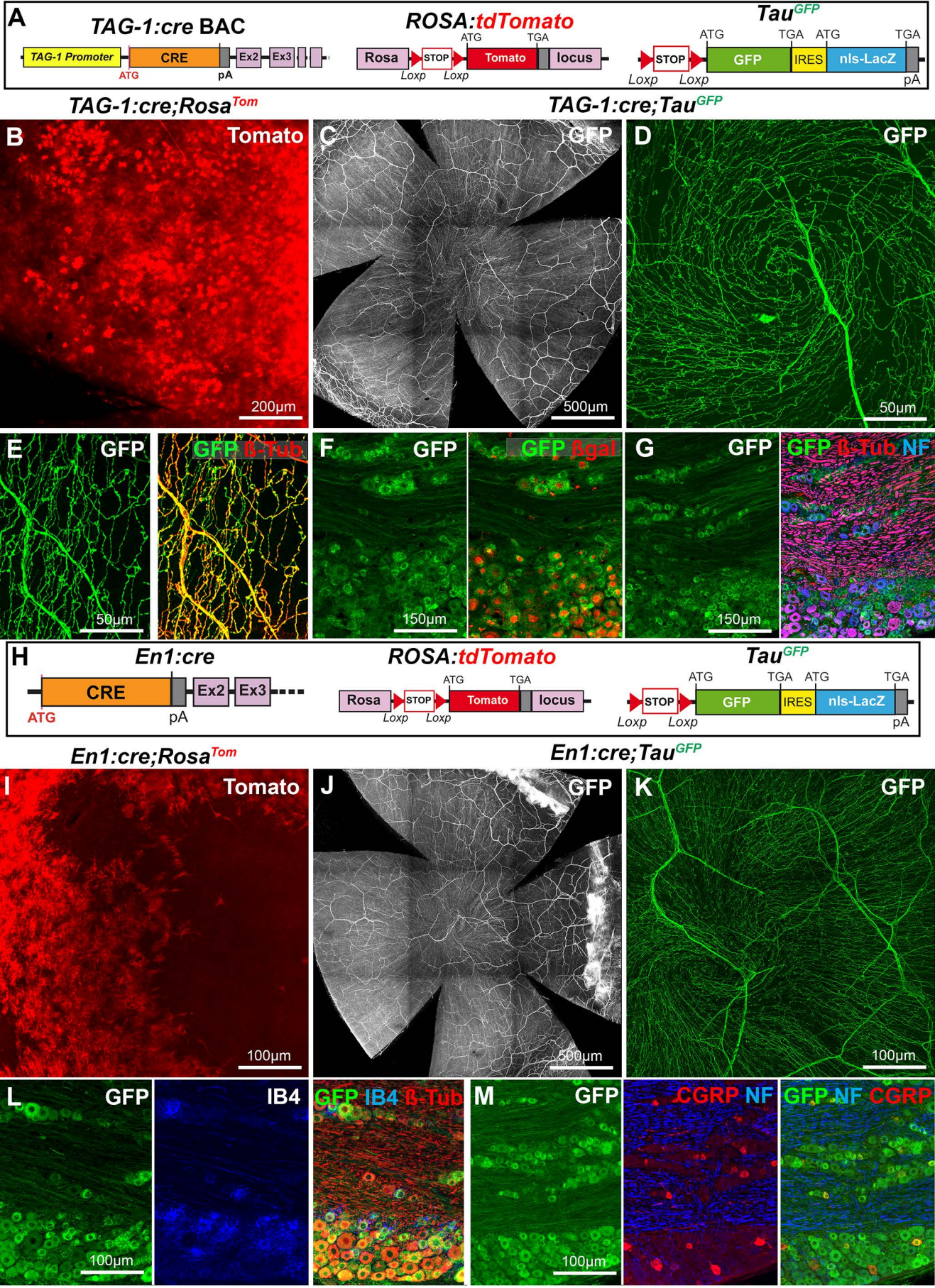
A
TAG-1:cre BAC
TAG-1 Promoter
CRE
Ex2
Ex3
ATG
pA
ROSA:tdTomato
Rosa
STOP
Tomato
locus
ATG
TGA
Loxp
Loxp
Tau GFP
STOP
GFP
IRES
nls-LacZ
ATG
TGA
ATG
TGA
Loxp
Loxp
pA
TAG-1:cre;Rosa Tom
TAG-1:cre;Tau GFP
B
Tomato
200µm
C
GFP
500µm
D
GFP
50µm
E
GFP
50µm
GFP ß-Tub
F
GFP
150µm
GFP ßgal
G
GFP
150µm
GFP ß-Tub NF
H
En1:cre
CRE
Ex2
Ex3
ATG
pA
ROSA:tdTomato
Rosa
STOP
Tomato
locus
ATG
TGA
Loxp
Loxp
Tau GFP
STOP
GFP
IRES
nls-LacZ
ATG
TGA
ATG
TGA
Loxp
Loxp
pA
En1:cre;Rosa Tom
En1:cre;Tau GFP
I
Tomato
100µm
J
GFP
500µm
K
GFP
100µm
L
GFP
100µm
IB4
GFP IB4 ß-Tub
M
GFP
100µm
CGRP NF
GFP NF CGRP

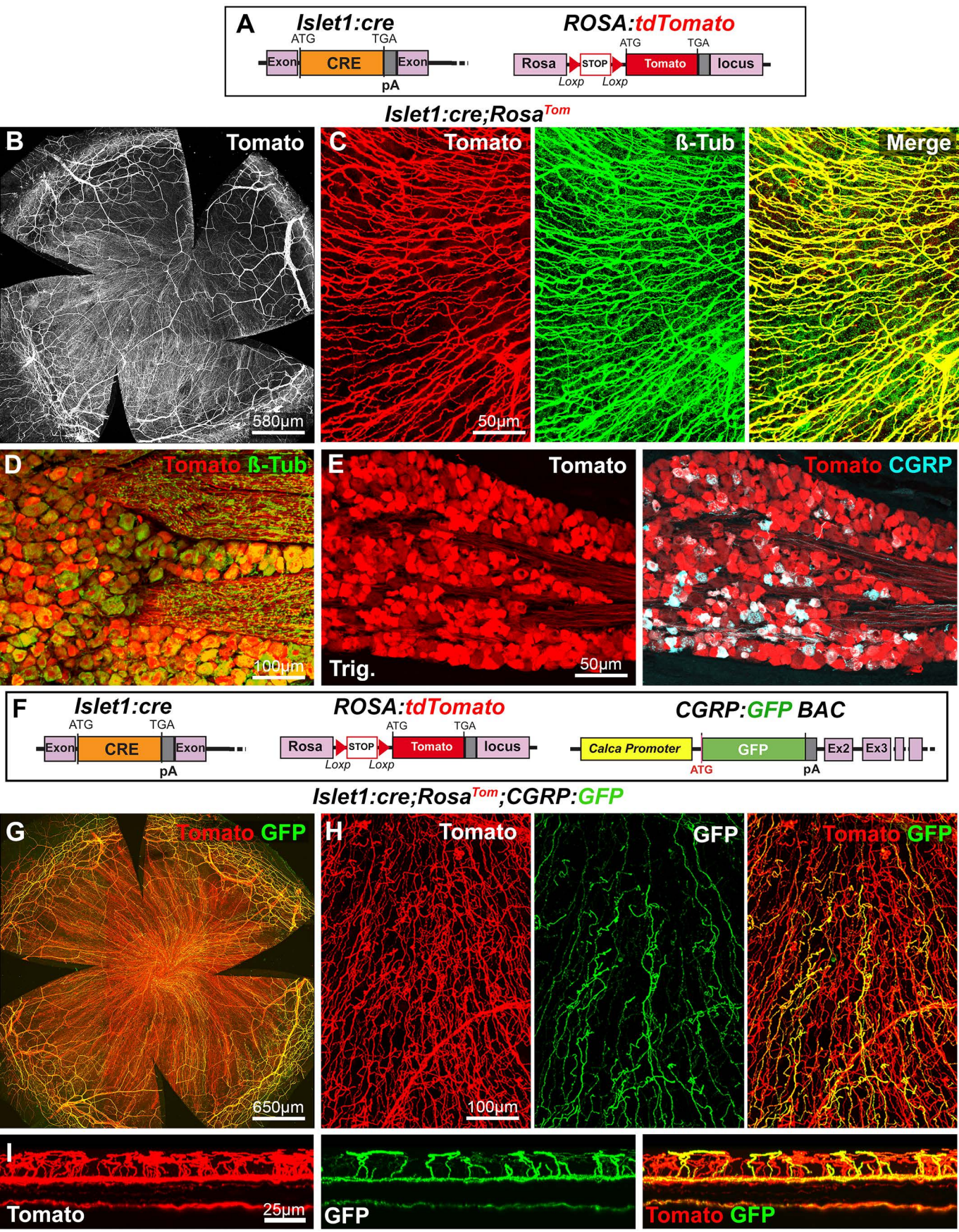
A
Islet1:cre
ATG
TGA
Exon
CRE
Exon
pA
ROSA:tdTomato
ATG
TGA
Rosa
STOP
Tomato
locus
Loxp
Loxp
Islet1:cre;Rosa Tom
B
Tomato
580µm
C
Tomato
50µm
ß-Tub
Merge
D
Tomato ß-Tub
100µm
E
Tomato
Trig.
50µm
Tomato CGRP
F
Islet1:cre
ATG
TGA
Exon
CRE
Exon
pA
ROSA:tdTomato
ATG
TGA
Rosa
STOP
Tomato
locus
Loxp
Loxp
CGRP:GFP BAC
Calca Promoter
GFP
Ex2
Ex3
ATG
pA
Islet1:cre;Rosa Tom ;CGRP:GFP
G
Tomato GFP
650µm
H
Tomato
100µm
GFP
Tomato GFP
I
Tomato
25µm
GFP
Tomato GFP

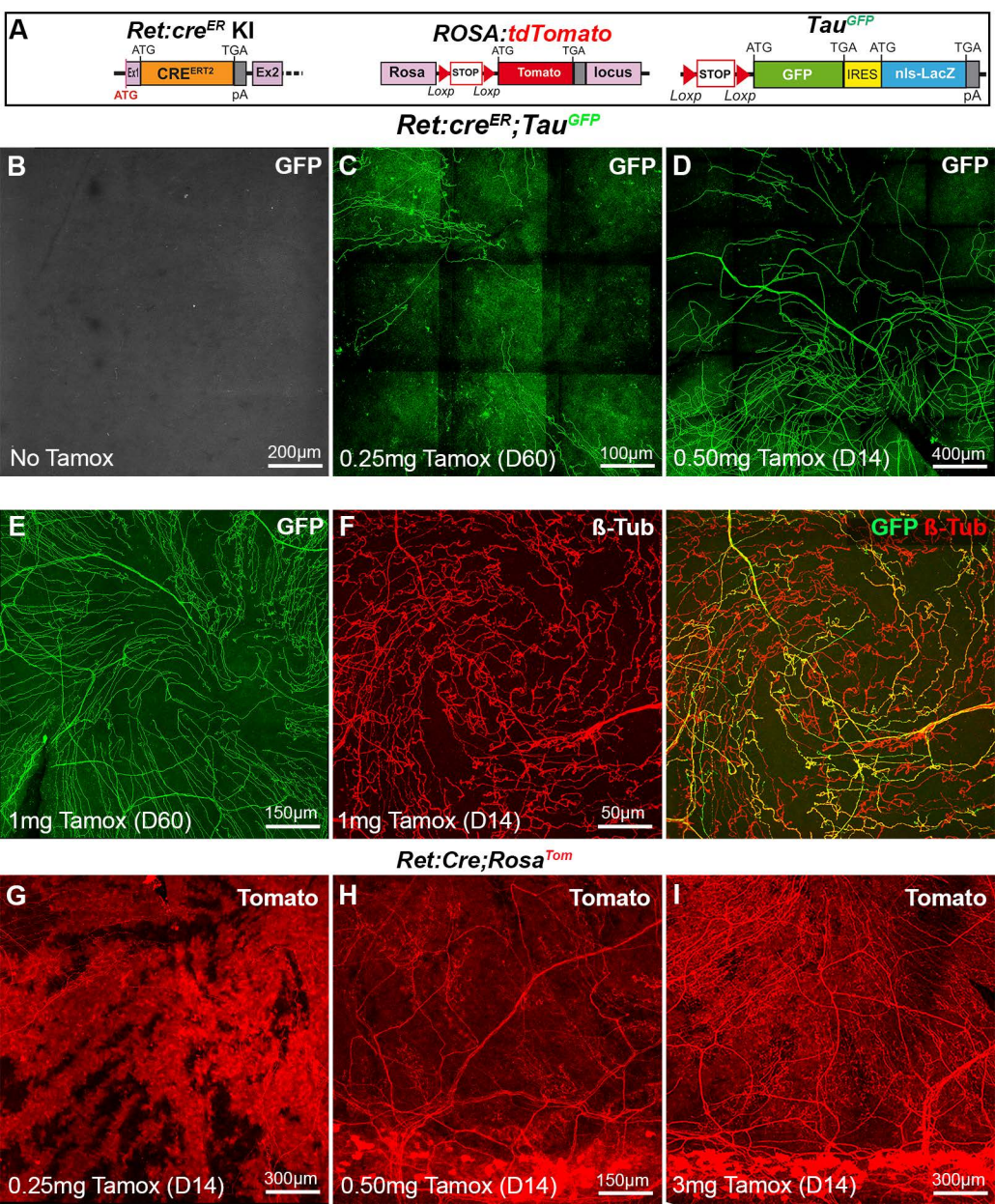
A
Ret:creER KI
ATG
TGA
Ex1
CRE ERT2
Ex2
ATG
pA
ROSA:tdTomato
ATG
TGA
Rosa
STOP
Tomato
locus
Loxp
Loxp
TauGFP
ATG
TGA
ATG
TGA
STOP
GFP
IRES
nls-LacZ
Loxp
Loxp
pA
Ret:creER;TauGFP
B
GFP
No Tamox
200µm
C
GFP
0.25mg Tamox (D60)
100µm
D
GFP
0.50mg Tamox (D14)
400µm
E
GFP
1mg Tamox (D60)
150µm
F
ß-Tub
1mg Tamox (D14)
50µm
GFP ß-Tub
Ret:Cre;RosaTom
G
Tomato
0.25mg Tamox (D14)
300µm
H
Tomato
0.50mg Tamox (D14)
150µm
I
Tomato
3mg Tamox (D14)
300µm

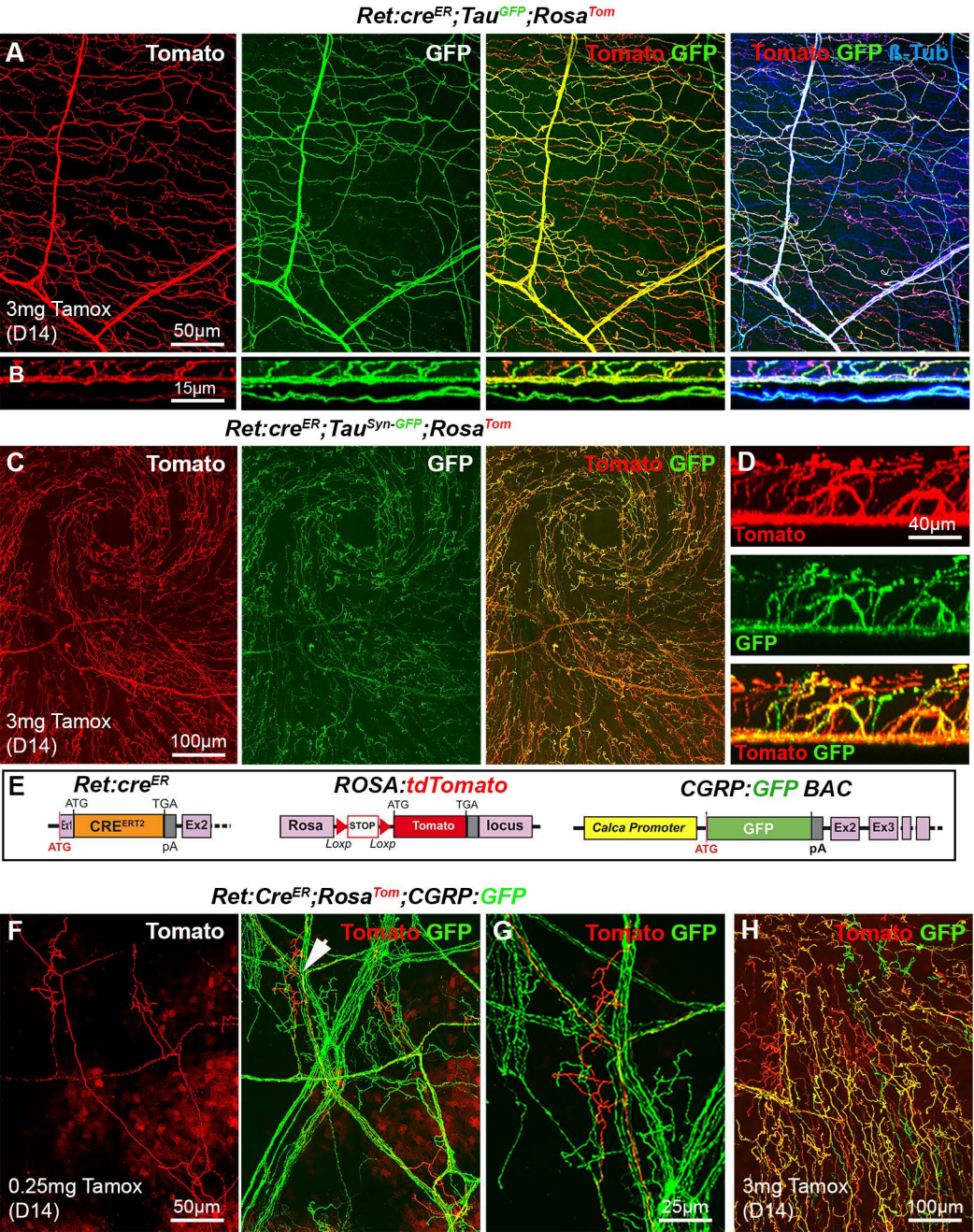
Ret:cre^ER;Tau^GFP;Rosa^Tom
A
Tomato
GFP
Tomato GFP
Tomato GFP ß-Tub
3mg Tamox
(D14)
50µm
B
15µm
Ret:cre^ER;Tau^Syn-GFP;Rosa^Tom
C
Tomato
GFP
Tomato GFP
3mg Tamox
(D14)
100µm
D
Tomato
40µm
GFP
Tomato GFP
E
Ret:cre^ER
ATG
TGA
Ex1
CRE^ERT2
Ex2
ATG
pA
ROSA:tdTomato
ATG
TGA
Rosa
STOP
Tomato
locus
Loxp
Loxp
CGRP:GFP BAC
Calca Promoter
GFP
Ex2
Ex3
ATG
pA
Ret:Cre^ER;Rosa^Tom;CGRP:GFP
F
Tomato
0.25mg Tamox
(D14)
50µm
Tomato GFP
G
Tomato GFP
25µm
H
Tomato GFP
3mg Tamox
(D14)
100µm

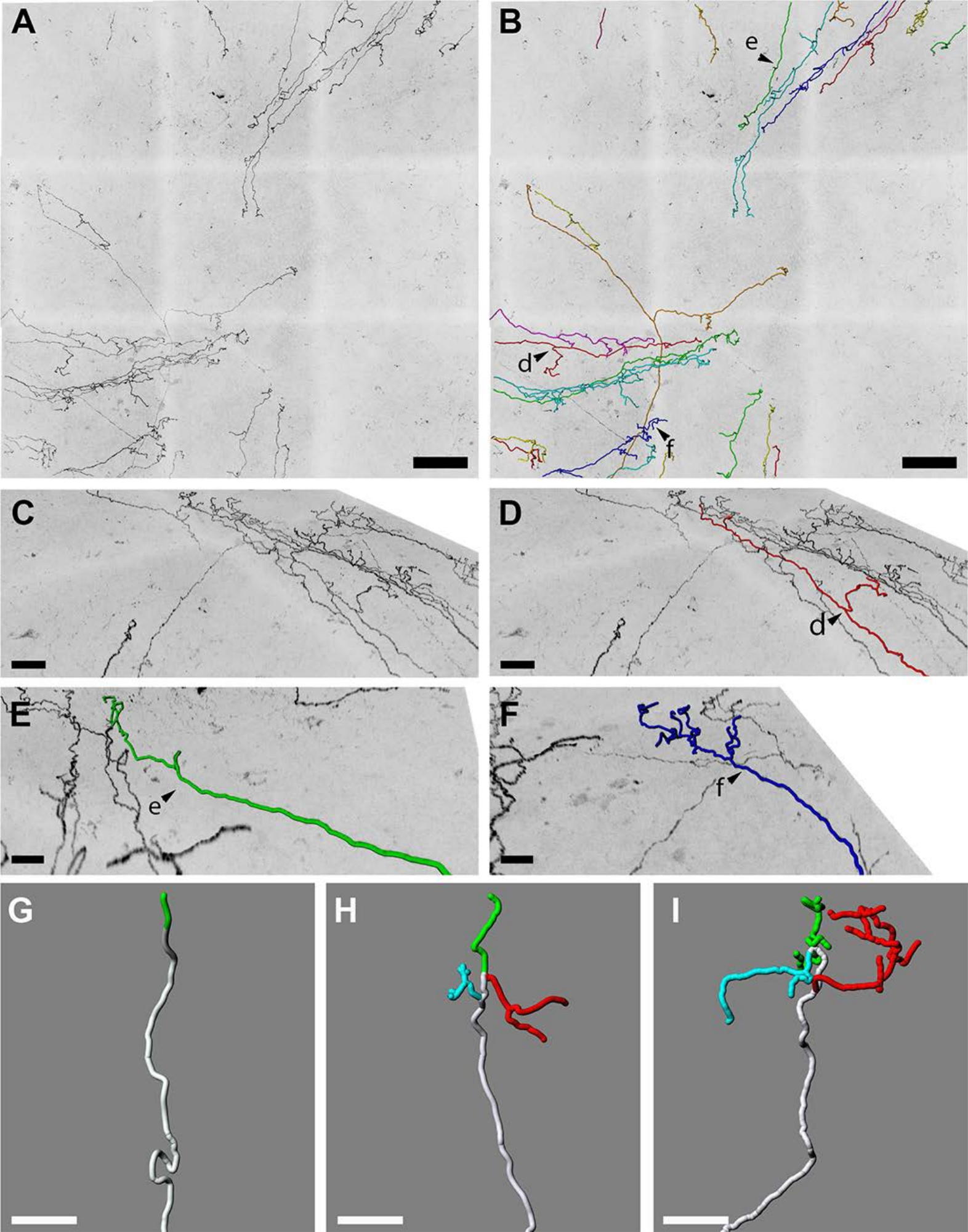
A
B
e
d
f
C
D
d
E
e
F
f
G
H
I

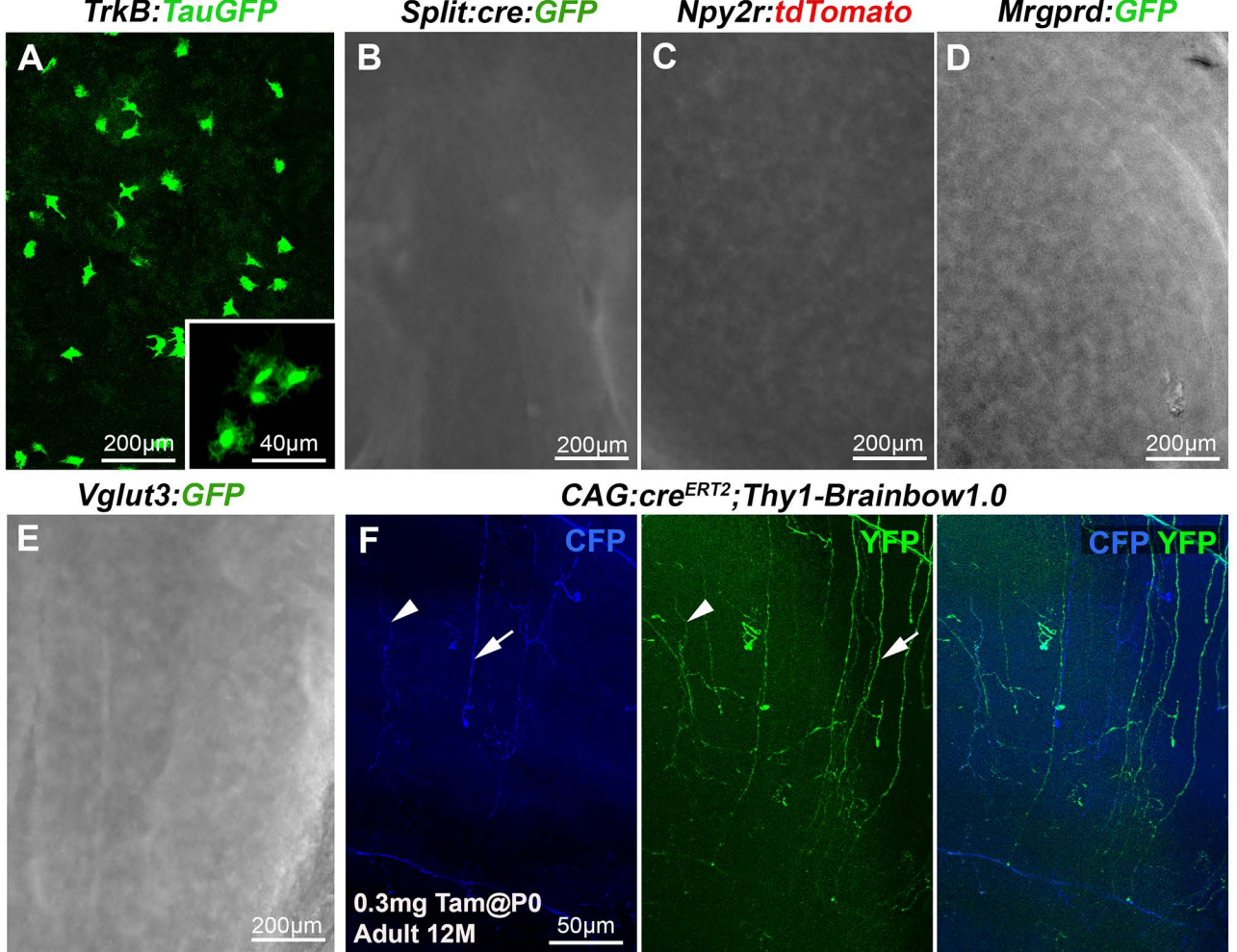
TrkB:TauGFP
Split:cre:GFP
Npy2r:tdTomato
Mrgprd:GFP
A
B
C
D
200μm
40μm
200μm
200μm
200μm
Vglut3:GFP
CAG:creERT2;Thy1-Brainbow1.0
E
F
CFP
YFP
CFP YFP
200μm
0.3mg Tam@P0
Adult 12M
50μm

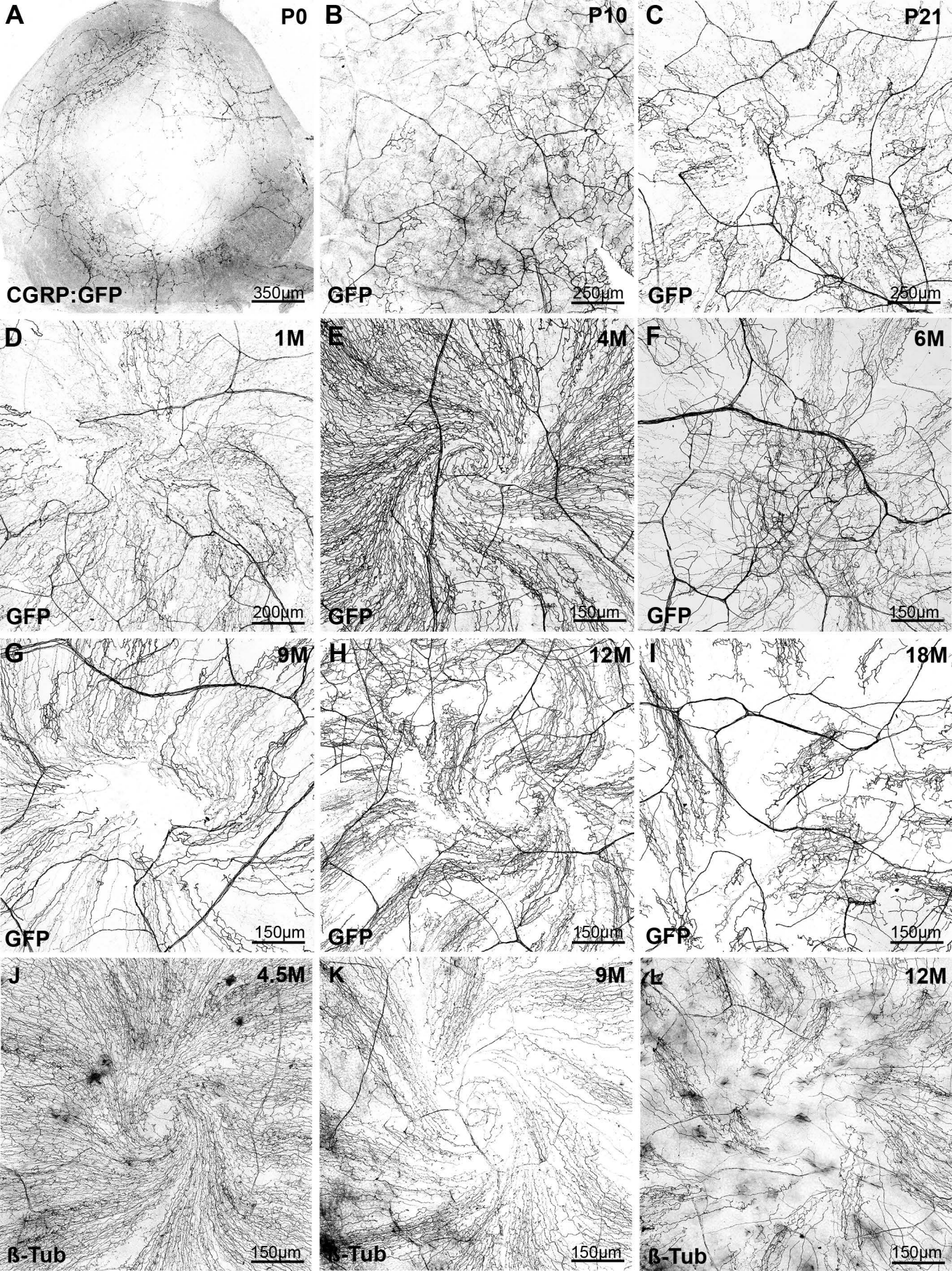
A
P0
CGRP:GFP
350µm
B
P10
GFP
250µm
C
P21
GFP
250µm
D
1M
GFP
200µm
E
4M
GFP
150µm
F
6M
GFP
150µm
G
9M
GFP
150µm
H
12M
GFP
150µm
I
18M
GFP
150µm
J
4.5M
ß-Tub
150µm
K
9M
ß-Tub
150µm
L
12M
ß-Tub
150µm

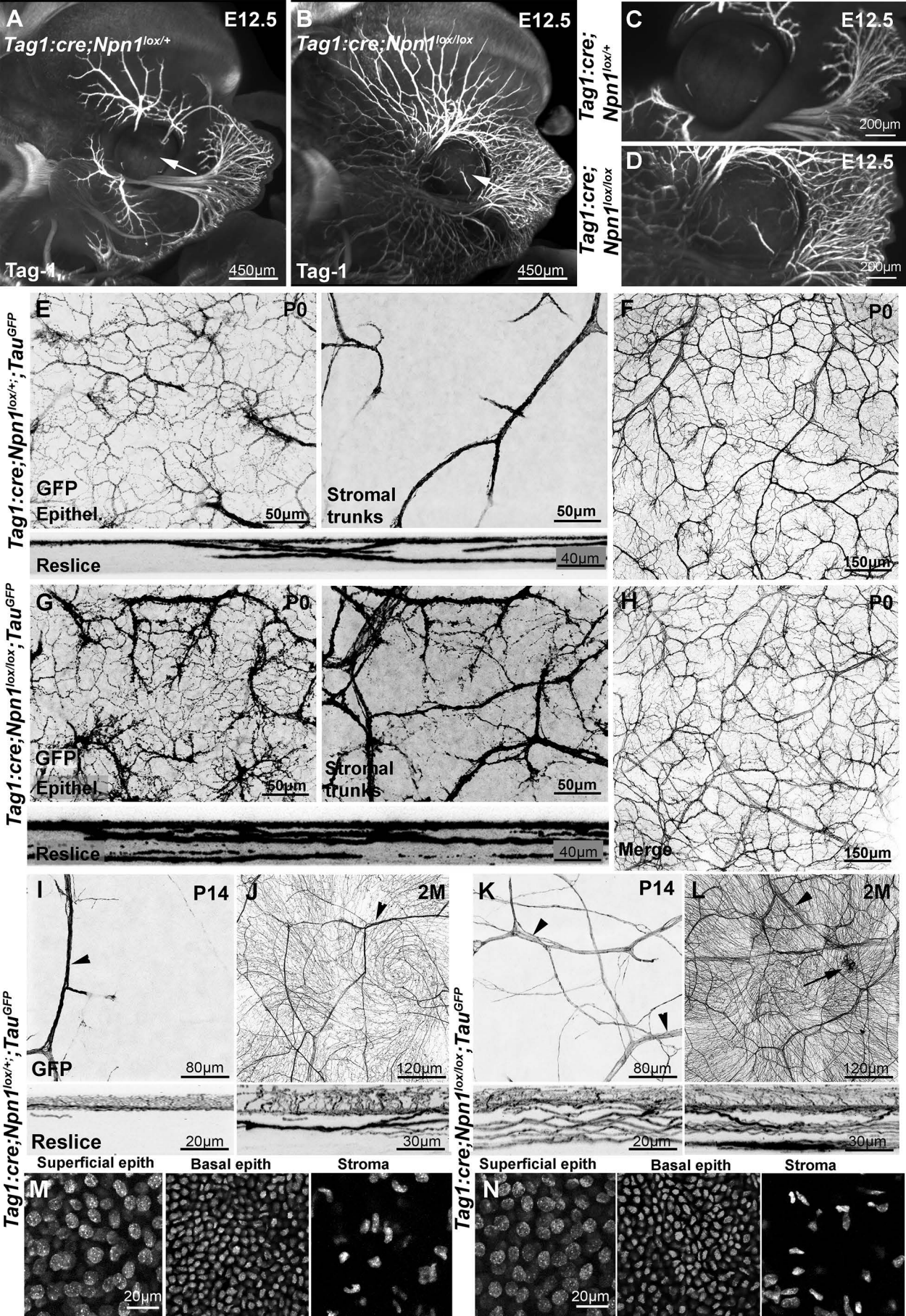
A
E12.5
Tag1:cre;Npn1lox/+
Tag-1
450µm
B
E12.5
Tag1:cre;Npn1lox/lox
Tag-1
450µm
C
E12.5
Tag1:cre; Npn1lox/+
200µm
D
E12.5
Tag1:cre; Npn1lox/lox
200µm
E
P0
GFP
Epithel.
50µm
Stromal trunks
50µm
Reslice
40µm
F
P0
150µm
Tag1:cre;Npn1lox/+;Tau GFP
G
P0
GFP
Epithel.
50µm
Stromal trunks
50µm
Reslice
40µm
H
P0
Merge
150µm
Tag1:cre;Npn1lox/lox;Tau GFP
I
P14
GFP
80µm
Reslice
20µm
J
2M
120µm
30µm
K
P14
80µm
20µm
L
2M
120µm
30µm
Tag1:cre;Npn1lox/+;Tau GFP
Tag1:cre;Npn1lox/lox;Tau GFP
Superficial epith
Basal epith
Stroma
M
20µm
N
20µm

Table 1: **Primary and secondary antibodies used.**

	Host	Vendor	Catalog no. (RRID no.)	Concentration
Primary antibodies				
Anti–βIII-tubulin	Rabbit	Covance	PRB-435P-100 (AB_291637)	1:1000
Anti-CGRP	Rabbit	Peninsula	T-4032 (AB_2313775)	1:1000
Anti-GFP	Rabbit	Invitrogen	A-11122 (AB_221569)	1:1000
Anti-βgal	Rabbit	MP Biochemicals	ab6645 (AB_2313831)	1:500
IB4		Sigma	L2140 (AB_2313663)	1:100
Anti-NF200	Chicken	Aves Labs	NF-H (AB_2313552)	1:1000
Anti-Tag-1	Goat	RD Systems	AF1714 (AB_2245173)	1:1000
Secondary antibodies				
Anti-rabbit Cy-2	Donkey	Jackson Laboratories	711-485-152 (AB_2492289)	1:500
Anti-rabbit Cy-3	Donkey	Jackson Laboratories	711-166-152 (AB_2313568)	1:500
Anti-rabbit Cy-5	Donkey	Jackson Laboratories	711-175-152 (AB_2340607)	1:500
Anti-rabbit Cy-2	Donkey	Invitrogen	A-21206 (AB_141708)	1:500
Anti-rabbit Cy-3	Donkey	Invitrogen	A-21207 (AB_141637)	1:500
Anti-rabbit Cy-5	Donkey	Invitrogen	A-31573 (AB_2536183)	1:500
Anti-goat Cy-2	Bovine	Jackson Laboratories	805-545-180 (AB_2340883)	1:500
Anti-goat Cy-3	Bovine	Jackson Laboratories	805-165-180 (AB_2340880)	1:500
Anti-goat Cy-5	Bovine	Jackson Laboratories	805-605-180 (AB_2340885)	1:500
Anti-chicken Cy-2	Donkey	Jackson Laboratories	703-545-155 (AB_2340375)	1:500
Anti-chicken Cy-3	Donkey	Jackson Laboratories	703-165-155 (AB_2340363)	1:500
Anti-chicken Cy-5	Donkey	Jackson Laboratories	703-175-155 (AB_2340365)	1:500
Alexa Cy-2 conjugated IB4		Thermo Fisher Scientific	S11223 (AB_2336881)	1:500

Table 2: Sample sizes for each experimental procedure.

Experimental procedure	Associated figure	Sample size (n)
Subset of trigeminal neurons expressing GFP	Figure 1F	5
Subset of corneal axons expressing GFP	Figure 1G	3
Corneal axons tracing	Figure 7	10
CGRP axons and aging	Figure 9	5 (4 months); 5 (12 months); 5 (18 months)
Neuropilin 1 and trigeminal development (E13)	Figure 10	3 mutants and 3 controls
Neuropilin 1 and corneal nerve development	Figure 10	3 (E13); 3 (P0); 3 (P14); 3 (2months) and 3 controls (E13; P0; P14; 2 months)